U.S.NRC

United States Nuclear Regulatory Commission

Protecting People and the Environment

Assessment of the Performance of the Extremely Low Probability of Rupture Code in an International Benchmark with Insights from Advanced Finite Element Analysis

Date:

August 22, 2023

Prepared in response to the Office of Nuclear Reactor Regulation User Need Request NRR-2021-008, Task 7, by:

E. Kurth-Twombly
Engineering Mechanics Corporation of Columbus

F. W. Brust
Engineering Mechanics Corporation of Columbus

C. J. Sallaberry
Engineering Mechanics Corporation of Columbus

R. Kurth
Engineering Mechanics Corporation of Columbus

NRC Project Manager:

Matthew Homiack
Materials Engineer
Reactor Engineering Branch

Division of Engineering
Office of Nuclear Regulatory Research
U.S. Nuclear Regulatory Commission
Washington, DC 20555–0001

DISCLAIMERS

This report was prepared as an account of work sponsored by an agency of the U.S. Government. Neither the U.S. Government nor any agency thereof, nor any employee, makes any warranty, expressed or implied, or assumes any legal liability or responsibility for any third party's use, or the results of such use, of any information, apparatus, product, or process disclosed in this publication, or represents that its use by such third party complies with applicable law.

This report does not contain or imply legally binding requirements. Nor does this report establish or modify any regulatory guidance or positions of the U.S. Nuclear Regulatory Commission and is not binding on the Commission.

Table of Contents

List of Tables

List of Figures

Acronyms

ADAMS	Agencywide Documents Access and Management System
AFEA	advanced finite element analysis
COD	crack opening displacement
Emc2	Engineering Mechanics Corporation of Columbus
FEA	finite element analysis
LBB	leak-before-break
LEAPOR	Leak Analysis of Piping—Oak Ridge
NRC	U.S. Nuclear Regulatory Commission
PFM	probabilistic fracture mechanics
PROLOCA	Probability of Loss Of Coolant Accident
PROMETHEUS	Probabilistic Methods for Evaluating and Understanding Structures
SIF	stress intensity factor
TWC	through-wall crack
WRS	weld residual stress
xLPR	Extremely Low Probability of Rupture

EXECUTIVE SUMMARY

Probabilistic fracture mechanics (PFM) assessment supports risk-informed decision-making. In PFM, fracture models are incorporated into a dynamic, Monte Carlo simulation environment to generate component failure frequency estimates with quantified uncertainties. Extremely Low Probability of Rupture (xLPR) is a PFM code for piping applications developed by the U.S. Nuclear Regulatory Commission and the Electric Power Research Institute. Other PFM codes have been developed by others in Organisation for Economic Co-operation and Development member states; however, all the PFM codes have been designed using different models and assumptions because there are no internationally accepted standards. To understand the effects of the different modeling approaches, the metals sub-group of the Working Group on Integrity and Ageing of Components and Structures of the Committee on the Safety of Nuclear Installations of the Organisation for Economic Co-operation and Development's Nuclear Energy Agency initiated a project to benchmark PFM codes for piping applications.

The basic benchmark problem was defined as a fictitious butt-weld fabricated from a nickel-based alloy commonly called "Alloy 182" in a pressurized-water reactor coolant system. The weld was subject to normal operating loads (e.g., pressure, deadweight, and thermal expansion) and weld residual stress (WRS) imposed during fabrication. A single, inside surface-breaking crack was assumed to be present in the weld and oriented circumferentially with an idealized, semi-elliptical shape. The crack growth mechanism was primary water stress corrosion cracking. The problem was analyzed with two different WRS profiles, which are a key drivers of primary water stress corrosion cracking.

Because PFM codes must employ some simplified models for computational efficiency, they may produce results that are different from more accurate finite element analysis approaches. Therefore, this study leveraged advanced finite element analysis (AFEA) results to assess the xLPR code's performance in the international PFM code benchmark study. Assessment of the xLPR code's performance relative to the other PFM codes and AFEA results is intended to guide future maintenance and development needs to ensure that the xLPR code is consistent with or leads the state-of-practice.

Comparisons with the AFEA results highlighted the importance of WRS on crack shape development, which is consistent with the observations made from comparisons of the PFM code predictions. Because the AFEA procedure determined the stress intensity factors (SIFs) at every point along the crack front, and then used those values to determine crack growth over time at each node point, it was possible to develop a crack shape different than the basic crack shapes supported by xLPR and the other PFM codes. The PFM codes typically assume an idealized crack shape and permit crack growth only at the deepest and surface points of the crack. This assumption forces the crack to remain semi-elliptical in shape rather than attain the natural crack evolution shape predicted by AFEA. With a linear WRS profile, there were no major differences among the results from xLPR and most of the other PFM codes and AFEA. However, with a more complex third-order polynomial WRS profile, the idealized crack shape

assumptions used by xLPR and most of the other PFM codes introduced more errors compared to the AFEA results. In such cases, it is possible that the estimation of the SIFs at additional locations around the crack front could produce results that are closer to the AFEA predictions.

The xLPR code generally performed well relative to the AFEA and other PFM codes involved in the benchmark study. Accordingly, within the parameters of these studies, the xLPR code is consistent with the state of practice. Assessing the extent to which the xLPR code may lead the state of practice is more difficult because of the constraints of the benchmark study. For instance, WRS has been shown to be critical in many of the results, and use of the universal weight function method allows the xLPR code to better represent a range of potential WRS profiles. However, to accommodate the capabilities of all the PFM codes involved in the benchmark study, only linear and third-order polynomial WRS profiles were considered. A benchmark problem with a realistic, nonpolynomial WRS profile could reveal the versatility of xLPR relative to other PFM codes.

1   INTRODUCTION

A host of probabilistic fracture mechanics (PFM) codes have been developed within the Organisation for Economic Co-operation and Development member states during the last four decades to support the continued safe operation of aging nuclear power plant components. Since there are no internationally accepted PFM standards, these PFM codes have been developed using different models and assumptions. To understand the effects of the diverse modeling approaches on the results of the different PFM codes, the metals sub-group of the Working Group of Integrity and Ageing of Structures of the Committee on the Safety of Nuclear Installation of the Organisation for Economic Co-operation and Development's Nuclear Energy Agency initiated a project to benchmark PFM codes for piping applications. The scope of that benchmarking project involves 14 PFM codes from as many participating organizations. The U.S. Nuclear Regulatory Commission (NRC)'s Office of Nuclear Regulatory Research participated in the benchmark project with the Extremely Low Probability of Rupture (xLPR) code. The benchmark project consists of three main phases: (1) questionnaire on PFM code design, (2) deterministic benchmark cases, and (3) probabilistic benchmark cases.

In xLPR code development, the NRC's Office of Nuclear Regulatory Research aims to be consistent with or lead the state-of-practice. Therefore, the results from the various phases of the benchmark have been assessed to determine the extent to which the xLPR code's current capabilities and performance are consistent with, lag, or lead the state-of-practice. This assessment will guide future xLPR code maintenance and development needs.

The results from the deterministic benchmark cases provide insights into the effects of different modeling choices on the leak-before-break (LBB) behavior of the selected benchmark problem, which analyzed the degradation mechanism primary water stress corrosion cracking. Three deterministic benchmark problems were defined for the benchmark study: DP-01, DP-02, and DP-03. DP-01 included a simplistic, linear weld residual stress (WRS) profile. DP-02 included a more complex WRS profile defined by a third-order polynomial. DP-03 omitted WRS altogether.

To inform the assessment of the xLPR code's performance in the benchmark study, two finite element analyses (FEAs) were performed based on the specifications for DP-01 and DP-02 as summarized by Homiack [1]. The FEAs naturally grew a crack using the advanced finite element analysis (AFEA) procedure described by Shim, et al. [2]. Using this procedure, the following set of parameters were determined from the simulated crack growth:

  (1)   stress intensity factors (SIFs) along the entire crack front including at the deepest and surface points

  (2)   crack opening displacements (CODs), including the effect of WRS

  (3)   time of crack transition from a surface-breaking crack to a through-wall crack (TWC) and transition to an idealized TWC

(4)   critical crack size and time of pipe rupture

(5)   leak rates

For items (2) through (5), the AFEA values were compared to the PFM code results at the time of first leak, time of rupture, and halfway between these times. The critical crack size was determined from the AFEA results using two different methods. For a given crack size and shape, the overload was applied with both net section collapse and the J-integral obtained for the prediction of instability. The leak rate was inferred using the COD and crack length data from item (2) as inputs to the Leak Analysis of Piping—Oak Ridge (LEAPOR) code.

2 APPROACH

This section summarizes the basic AFEA model development and analysis procedure.

2.1 FEA Model Development

To aid in the assessment of differences among xLPR and the other PFM codes, two FEA models based on the benchmark specifications were developed: one for DP-01 with a linear WRS profile and the other for DP-02 with a third-order polynomial WRS profile. The benchmark problem focused on determining the LBB behavior of a nickel-based alloy dissimilar metal weld in a large-bore piping system of a pressurized water reactor. The weld geometry and loads are listed in Table 2-1. The two WRS profiles for DP-01 and DP-02 are given by Eq. 1 and Eq. 2, respectively, and are shown in Figure 2-1. The material properties of the weld material are shown in Table 2-2.

Table 2-1   Benchmark problem geometry and loading

Parameter	Value	Units
Outside diameter, D_o	380	mm
Wall thickness, t	40	mm
Initial crack half-length, c_i	3	mm
Initial crack depth, a	1.5	mm
Operating pressure, P	15.5	MPa
Axial membrane stress, σ_m	0.117	MPa
Primary bending stress, σ_b	30.05	MPa

$$\sigma_{WRS-1}(MPa) = -800\left(\frac{x}{t}\right) + 400 \qquad \text{Eq. 1}$$

$$\sigma_{WRS-2}(MPa) = -3591\left(\frac{x}{t}\right)^3 + 6804\left(\frac{x}{t}\right)^2 - 3496\left(\frac{x}{t}\right) + 378 \qquad \text{Eq. 2}$$

In Equations 1 and 2, x/t is the normalized depth through the wall thickness as measured from the inside diameter.
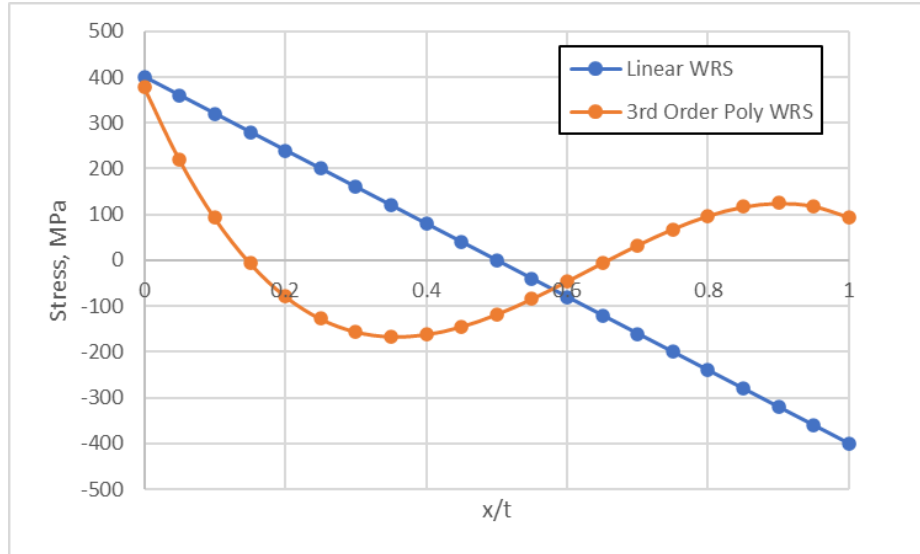
Figure 2-1   Linear and third-order polynomial WRS profiles for deterministic benchmark problems

Table 2-2   Benchmark problem material properties

Parameter	Value	Units
Yield strength, S_y	316.5	MPa
Ultimate strength, S_u	542.4	MPa
Modulus of elasticity, E	196,800	MPa
Reference strain, ε_o	0.001608	--
Reference stress, σ_o	316.5	MPa
Hardening modulus, α_{mat}	1.2436	--
Hardening exponent, n	5.5349	--

Using these parameters, a finite element mesh was developed using PipeFracCAE [3], which is a code developed at Engineering Mechanics Corporation of Columbus (Emc²) to create efficient crack meshes. Figure 2-2 shows the mesh created for both the DP-01 and DP-02 FEAs for the initial crack size and shape. The increased mesh refinement at the crack tip is shown magnified in the right-hand frame. The increased mesh refinement at the crack tip and along the crack front allows for accurate calculation of the SIFs at all nodes along the crack front as well as the additional crack contours. The SIFs are calculated at five crack contours to verify that the calculated values are independent of the mesh.

4
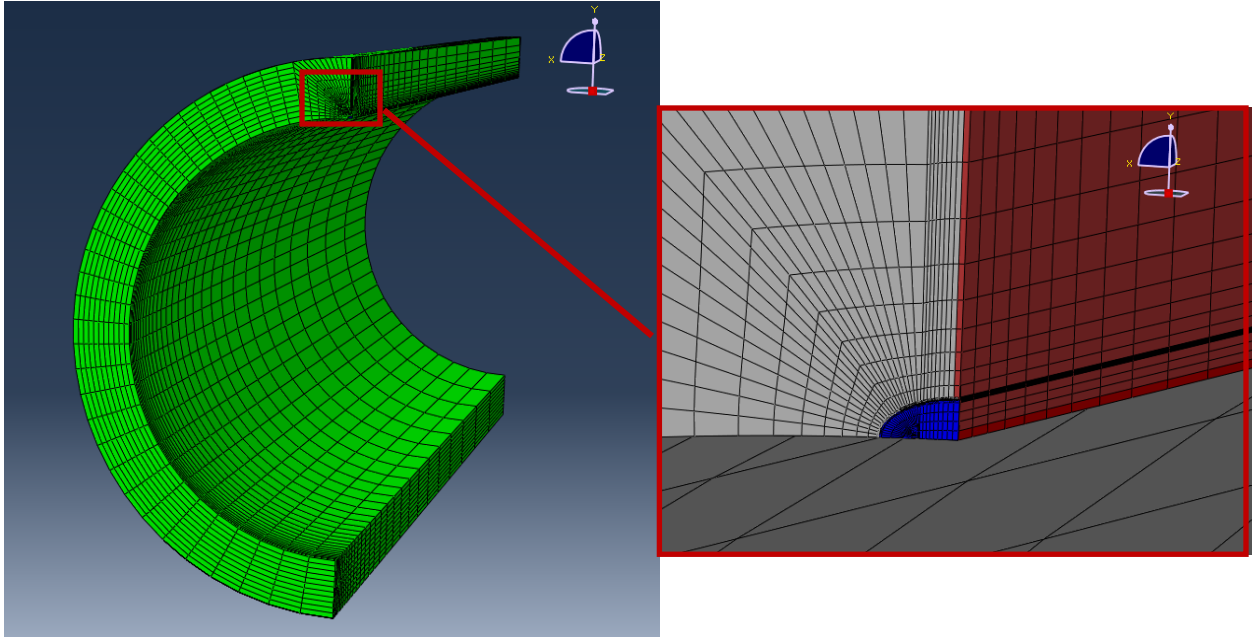
Figure 2-2   Finite element mesh for initial crack

2.2   Analysis Methods for WRS Inputs

The WRS is incorporated into the finite element mesh through a mapping procedure. The mapping is determined through a fitting procedure to determine the temperature field that corresponds to the specified WRS profile as described in Shim, et al. [2]. First, the crack is closed by tying together the nodes on the crack face so that the crack will not grow. Then, the temperature field is estimated as $T = \sigma_{WRS}/\alpha E$, where σ_{WRS} is the stress from the specified WRS profile at x/t, α is the coefficient of thermal expansion, and E is the modulus of elasticity. The analysis is run using this temperature field as the initial guess through the Emc²-developed *utemp* user subroutine that interfaces with the Abaqus software. The resulting stress is extracted from the results and then compared to the specified WRS profile. If the stress profiles are not similar, a correction to the temperature field is made based on the error from the previous iteration. This process is repeated until the resulting stress determined by FEA is considered close enough to the specified WRS profile by visual inspection. The procedure normally takes between 5 and 15 iterations, with each iteration resulting in a different finite element solution to be solved. The specified WRS profile, converged solution by FEA, and several intermediate solutions are shown to illustrate the process in Figure 2-3 for DP-01 and in Figure 2-4 for DP-02. It took nine iterations to develop a reasonable solution for the linear WRS profile in DP-01 and eight iterations for the nonlinear WRS profile in DP-02. Use of the temperature field to mimic the WRS field is a convenient way to impose the secondary loads from WRS. Once the temperature field corresponding to the specified WRS field is determined, the nodes on the crack face are released to open the crack, and the AFEA procedure can be run.
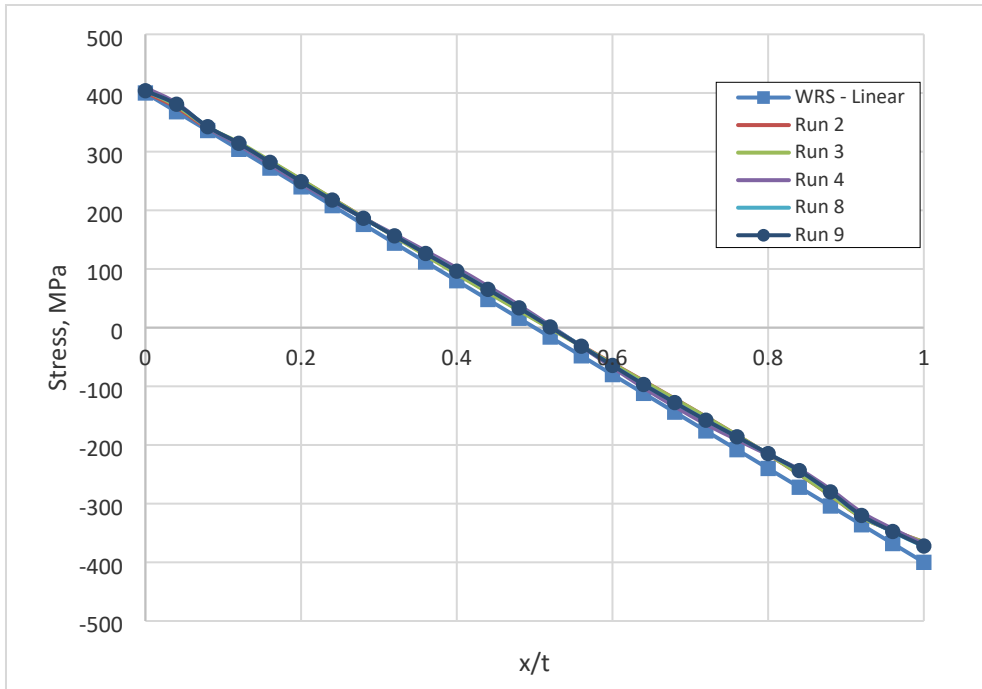
Figure 2-3 WRS profiles from FEA fitting procedure converging to the specified linear WRS profile for DP-01
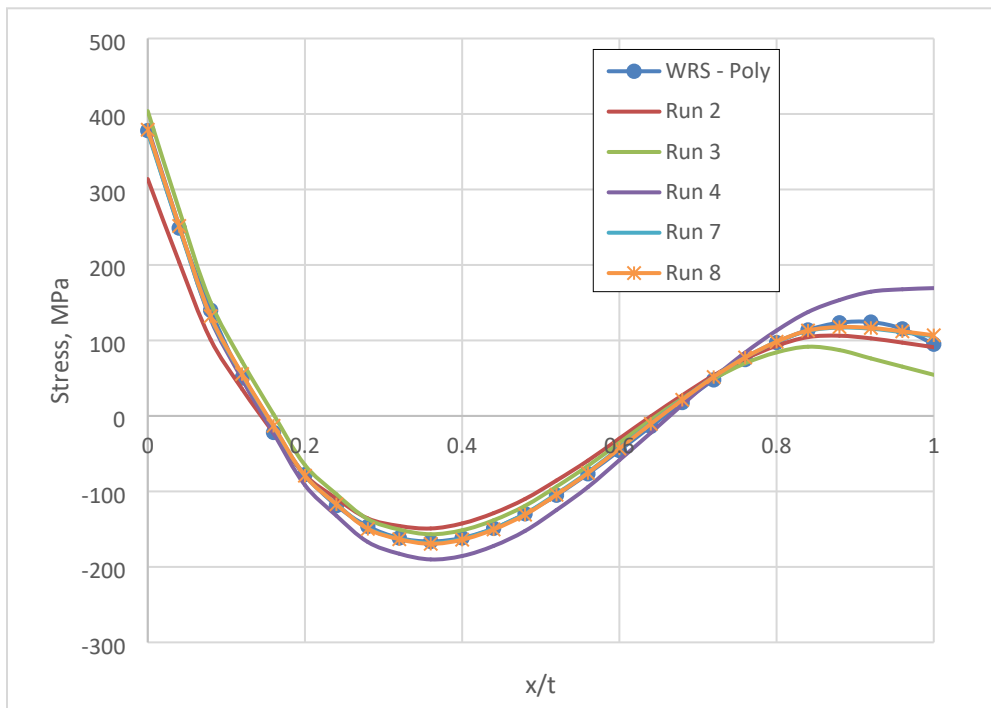
Figure 2-4 WRS profiles from FEA fitting procedure converging to the specified third-order polynomial WRS profile for DP-02

The AFEA procedure allows the crack to grow "naturally." That is, the SIFs along the entire crack front are determined and used to calculate the growth at each node. This approach is different than growing the crack elliptically, such as in the xLPR code, where only the SIFs at the crack inside surface and depth points are used to calculate crack growth and an elliptical shape is assumed to connect the points. The AFEAs for DP-01 and DP-02 were run using the Emc2-developed mesh generator, PipeFracCAE, and Abaqus. PipeFracCAE generates the mesh, which Abaqus then uses to perform the FEA. The SIFs are read from the Abaqus output file, crack growth at each node along the crack front is calculated, and then the new crack front nodes are read back into PipeFracCAE to regenerate the mesh with the larger crack size. This process is repeated until rupture occurs or crack growth ceases.

Although the natural crack growth process is relatively simple in terms of the number of steps performed, the finite element procedure and mesh is quite complex. The mesh needed for accurate results, especially at the crack tip, often requires hundreds of thousands of elements and nodes. Due to the different crack growths at different nodes along the crack front, which depend on the local SIF values, automatic meshing of such complex geometries is challenging. The automatic crack growth and meshing process must be checked every few steps to ensure the validity of the mesh as described by Brust, et al. [4].

3 RESULTS AND DISCUSSION

This section presents the AFEA results for DP-01 and DP-02 and compares them to the predictions from xLPR and the other PFM codes involved in the benchmark study. The results include comparisons of the calculated crack depths, crack lengths, SIFs, CODs, leak rates, and critical crack sizes. Sections 3.1 through 3.6 present deterministic comparisons of these results. In Section 3.7, the AFEA results are compared along with the distributions from the probabilistic benchmark results.

3.1 Crack Depth

The crack depth as a function of time is an essential parameter in determining the risk that a crack poses to the integrity of a piping component. Accordingly, crack depth for the benchmark problems and the impact of the specified WRS on crack growth were examined.

3.1.1 DP-01 Crack Depth Comparisons

The crack depth as a function of time for DP-01 is shown in Figure 3-1. The crack transitions to a TWC at 25.85 months.
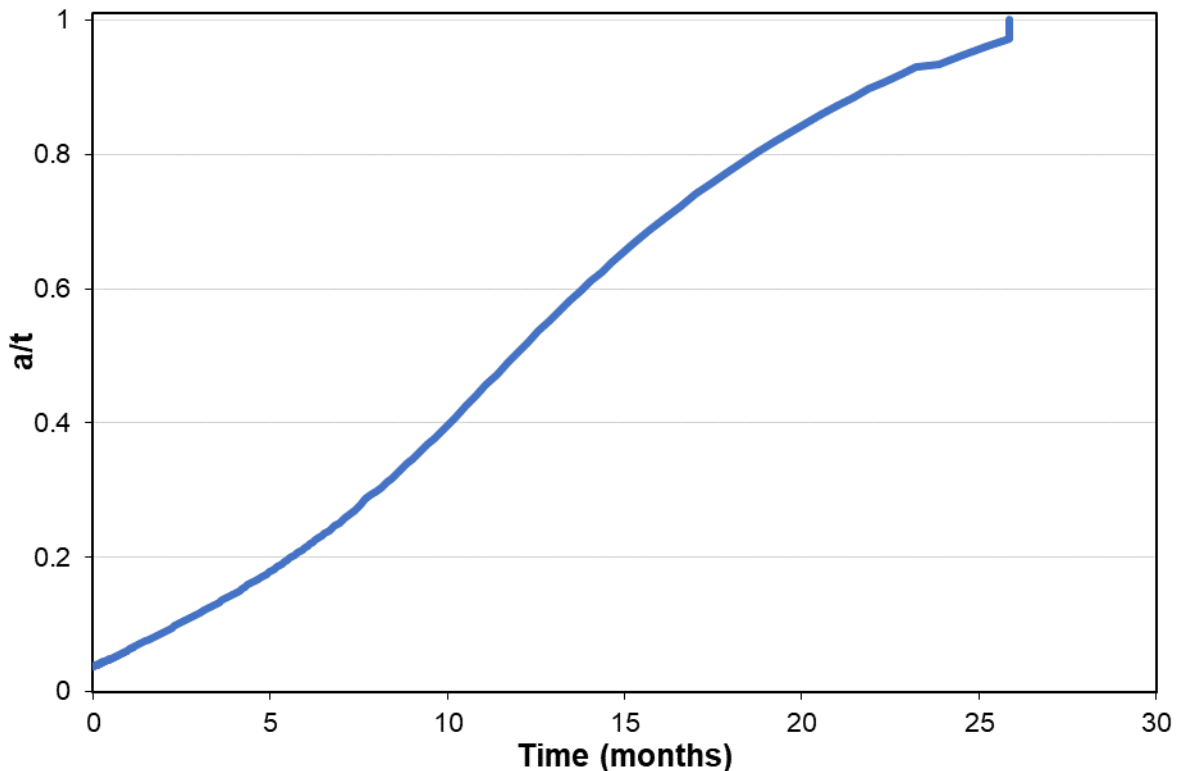
Figure 3-1   DP-01 normalized crack depth as a function of time (AFEA results)

The finite element mesh right before TWC transition, corresponding to a crack depth of $0.973t$, is shown in Figure 3-2(a), and the mesh shortly after becoming a TWC is shown in Figure

3-2(b). These results show that, for DP-01, as the crack grows through the pipe wall, it maintains an elliptical shape and looks like a transitioning crack as it becomes a TWC.

(a)   (b)
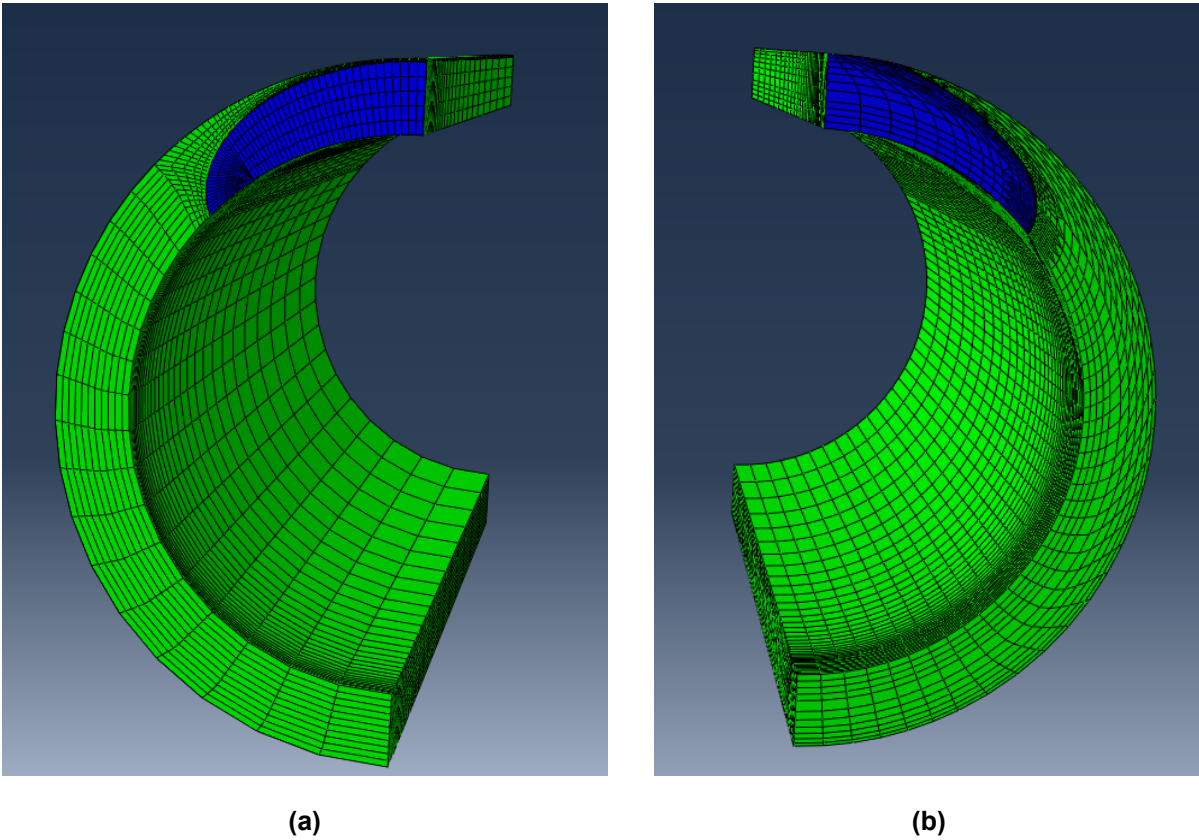
Figure 3-2   DP-01 finite element mesh (a) shortly before reaching TWC and (b) shortly after TWC formation

Figure 3-3 compares the crack depth determined by AFEA with the PFM code predictions. It shows that the crack growth determined by AFEA is slightly slower than the PFM codes. Then, beginning about halfway through the pipe wall, AFEA predicts slightly faster crack growth resulting in a time to TWC that is near the average of the PFM code predictions. Note that many of the PFM codes used a bounding depth value to transition from a surface crack to a TWC. For example, the transition point is set to $0.95t$ in the xLPR code and in most of the other PFM codes. The transition points are visible in Figure 3-3 by the vertical jumps in crack depth. The crack transition threshold seems reasonable given that the AFEA estimate was at $0.973t$.
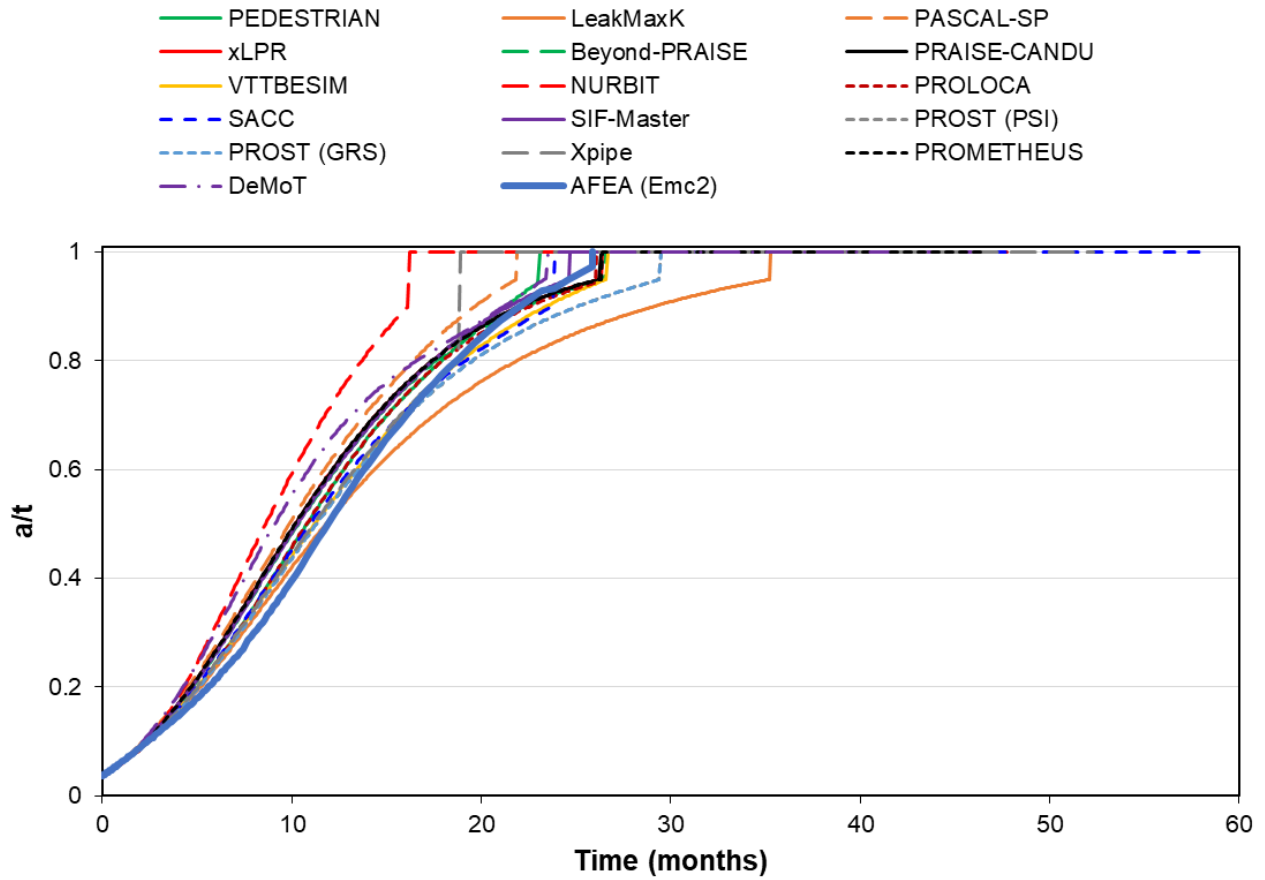
Figure 3-3   DP-01 AFEA crack depth compared to PFM code calculations

Looking specifically at the comparison between the xLPR code and AFEA predictions in Figure 3-4, both predict a nearly identical time to TWC. While there were some slight differences in the crack depth predictions, they were reasonably small.
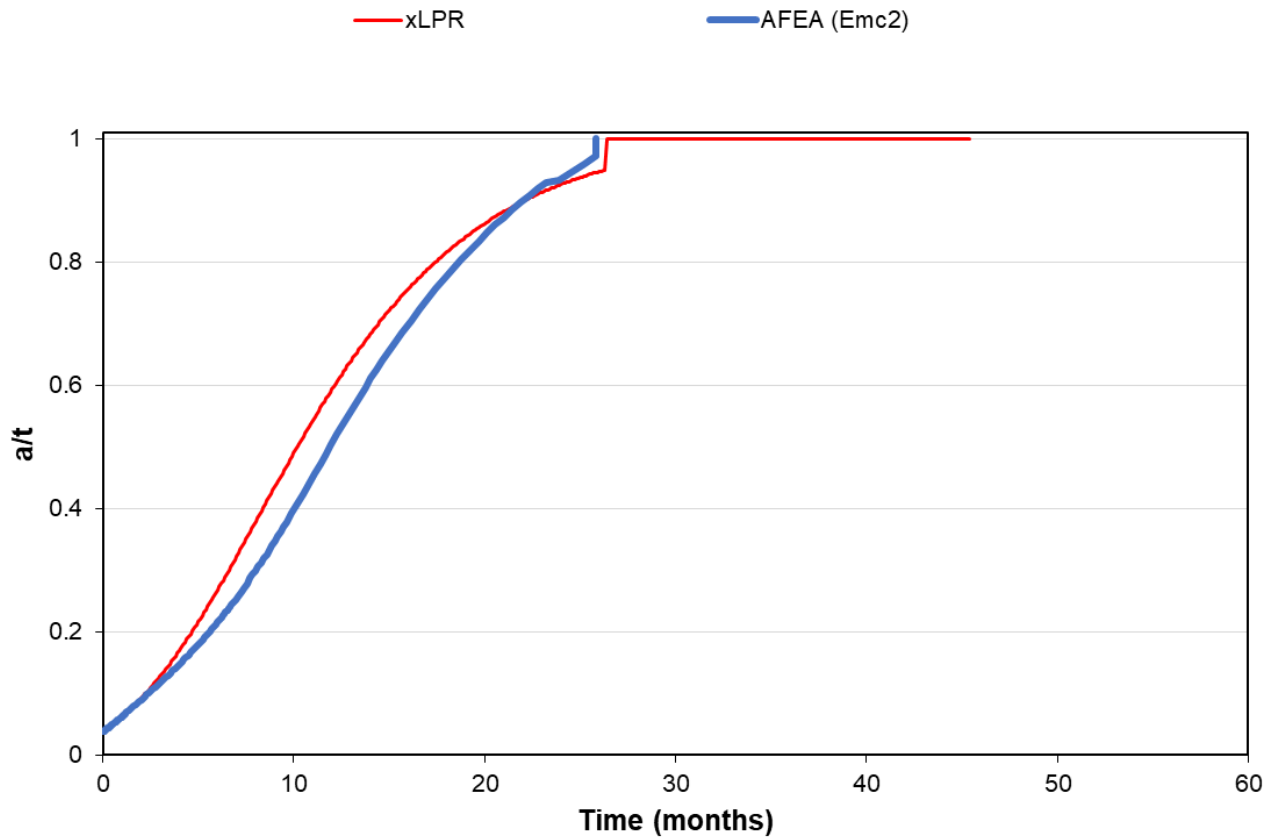
Figure 3-4   DP-01 AFEA crack depth compared to xLPR code calculations

3.1.2   DP-02 Crack Depth Comparisons

The AFEA estimation for crack depth as a function of time for DP-02 is shown in Figure 3-5. The crack transitioned to a TWC at 238 months. In examining the crack depth curve in Figure 3-5 along with the WRS profile for DP-02 shown in Figure 2-1, the impact of WRS on crack growth can be seen. For instance, the crack begins to grow more slowly according to Figure 3-5 at a little less than $0.4t$. The slower crack growth corresponds with the most compressive region of the WRS profile shown in Figure 2-1. Likewise, the crack begins to grow more rapidly just after $0.6t$, which corresponds to when the WRS profile becomes tensile again.
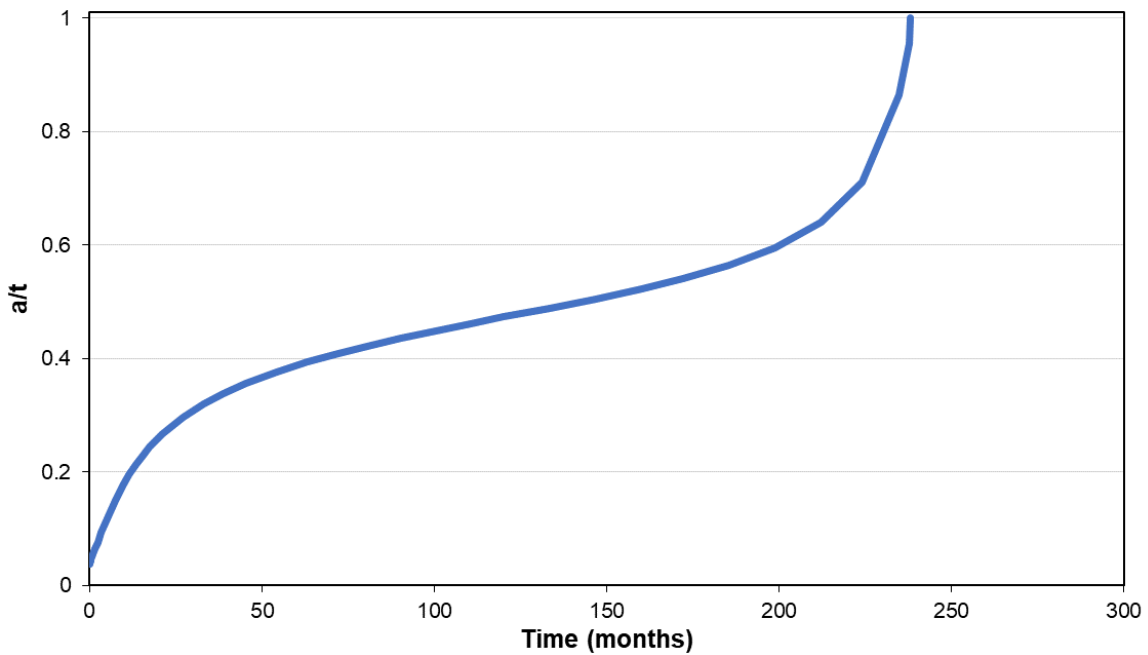
Figure 3-5   DP-02 normalized crack depth as a function of time (AFEA results)

Figure 3-6(a) displays the DP-02 finite element mesh right before TWC transition, corresponding to a crack depth of $0.956t$. Figure 3-6(b) shows the mesh shortly after TWC formation.

<div align="center">
(a)   (b)
</div>
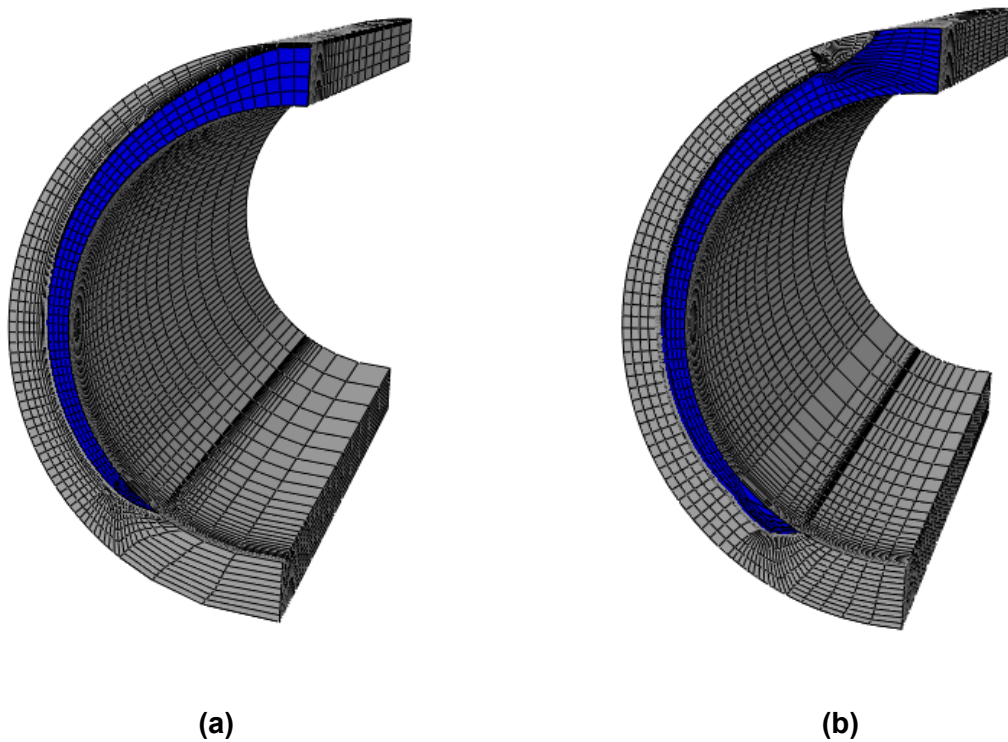
Figure 3-6   DP-02 finite element mesh of crack (a) shortly before reaching TWC and (b) shortly after TWC formation

Figure 3-7(a) shows the finite element mesh when the crack grew 360 degrees around the inside circumference, and Figure 3-7(b) shows the mesh at the critical crack size for DP-02. These meshes show that the crack shape remains complex (i.e., non-idealized) throughout its entire growth. The crack grew to 360 degrees around the inside circumference 38 months after becoming a TWC; the critical crack size was reached 12 months later.

(a) **(b)**
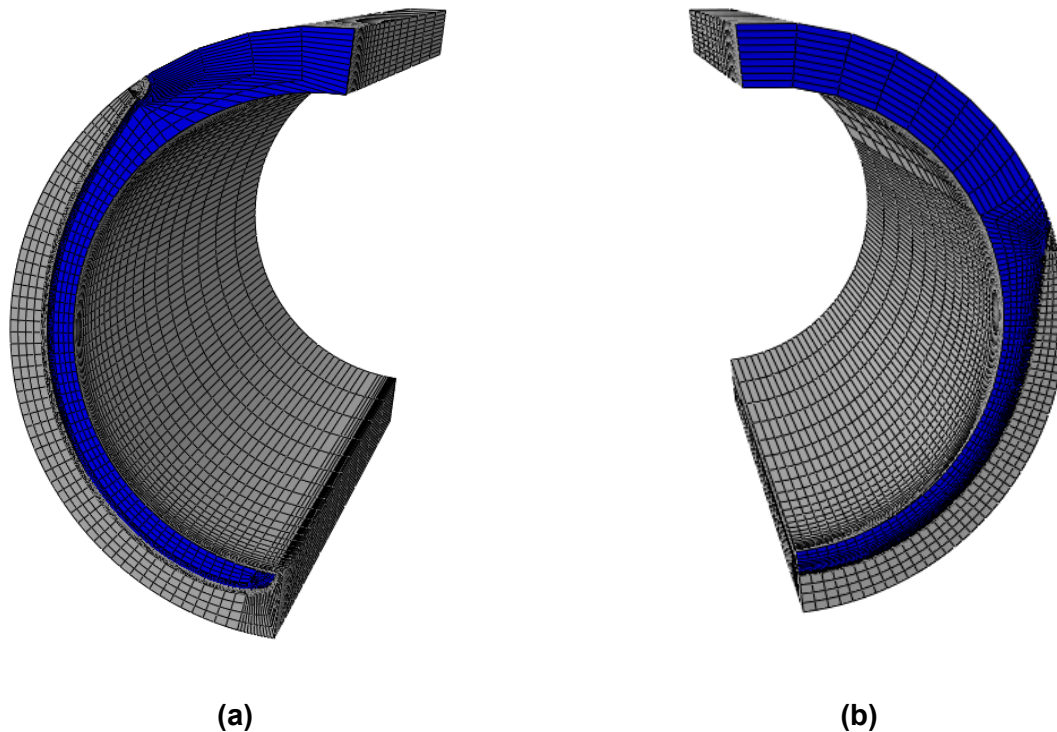
Figure 3-7   DP-02 finite element mesh of crack with (a) 360 degrees of growth on the inside diameter and (b) at the critical crack size

Figure 3-8 compares the crack depths for DP-02 determined by AFEA with the PFM code predictions. Figure 3-9 specifically compares the AFEA and xLPR code predictions. These figures show that the AFEA crack growth through the pipe wall thickness is essentially the same as all the PFM codes until approximately 40 months, or $0.35t$. These results coincide with the most compressive part of the WRS profile specified for DP-02. The compressive WRS field slows crack growth through the thickness more in the AFEA simulation than in many of the PFM codes, including xLPR. From Figure 3-8, the PFM code that most closely matches the AFEA prediction for crack depth is VTTBESIM. The differences in crack growth through the pipe wall thickness led to differences in the TWC times. The xLPR code predicted that the crack would become a TWC at about 174 months, whereas the AFEA prediction was 240 months. The natural crack growth process using AFEA is more realistic compared with the process used in most of the PFM codes, including the xLPR code, which assume crack growth only at the deepest and pipe-inside-surface points. The NURBIT code uses a different procedure, which attempts to model the elliptical crack shape evolution by averaging crack growth over the entire elliptical shape resulting in a modified, average crack growth. However, as shown in both Figure 3-3 for DP-01 and Figure 3-8 for DP-02, the NURBIT approach appears to produce results that are inconsistent with the AFEA results.

.
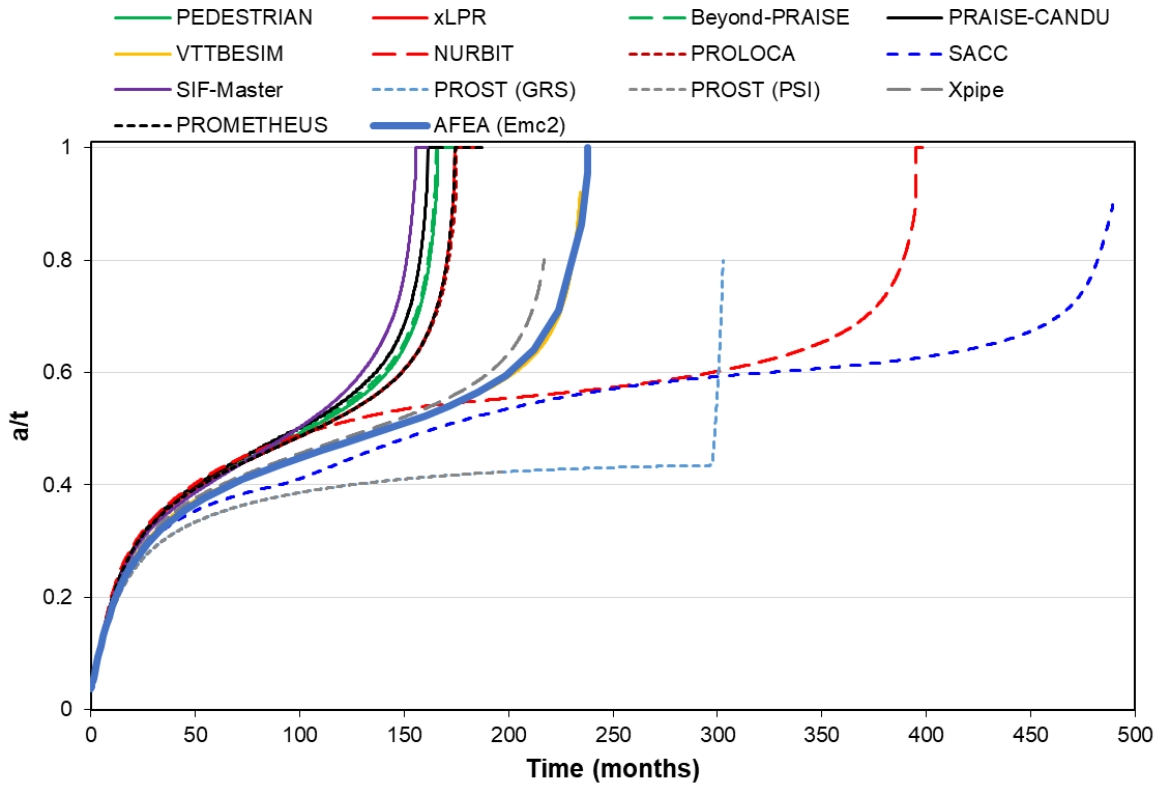
Figure 3-8   DP-02 AFEA crack depth compared to PFM code calculations
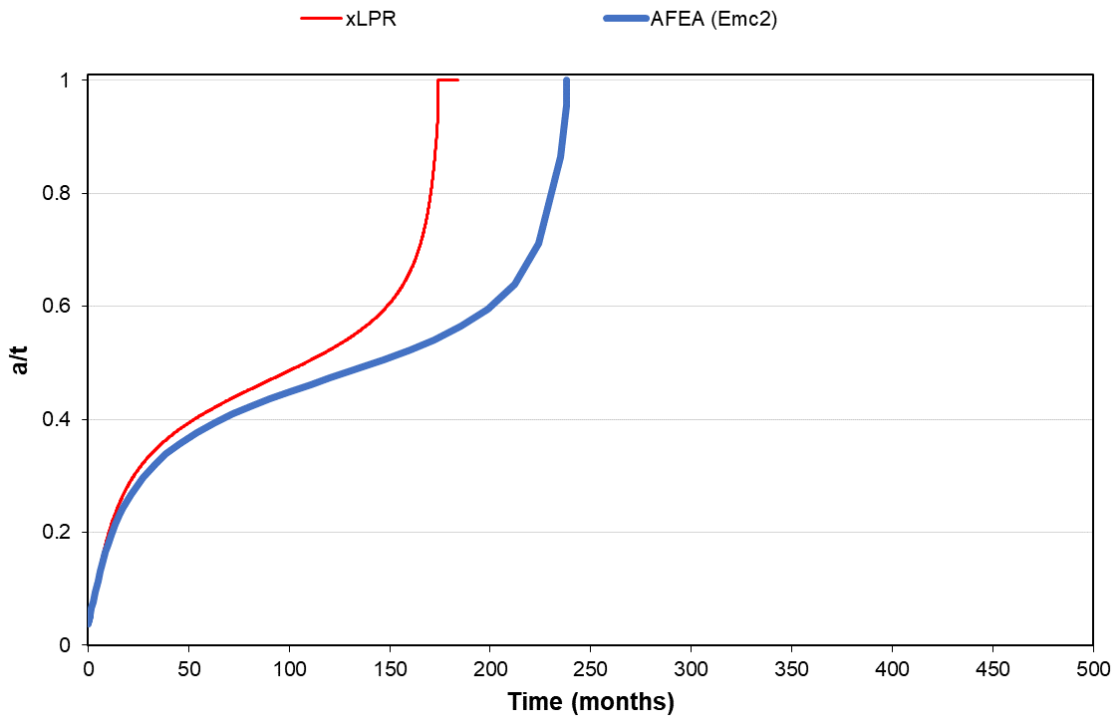
Figure 3-9   DP-02 AFEA crack depth compared to xLPR code calculations

3.2   Crack Length

The crack length as a function of time along the inside surface of the pipe is important in determining the shape of the crack as it transitions through-wall and then to an idealized TWC. A long, inside diameter crack length as the crack transitions through-wall can lead to a higher probability of break-before-leak due to an insufficient amount of time between crack or leak detection and subsequent intervention. The longer crack length gives a larger damaged area, which can make the crack closer to the critical crack size right before it becomes a TWC. This condition can lead to crack instability as soon as the crack penetrates through-wall. Once becoming a TWC, crack growth on the outside surface can be measured to determine how quickly the crack grows from a transitioning crack to an idealized TWC, and leak rates as a function of time can be calculated. Therefore, determining the likelihood of developing a long surface crack as well as the growth of a TWC are important in assessing the LBB behavior of piping components. Accordingly, crack growth along the inside and outside diameters and the impact of the WRS on crack growth were examined.

3.2.1   DP-01 Crack Length Comparisons

The inside and outside diameter normalized crack half-length angles, θ, for DP-01 as determined by AFEA are shown in Figure 3-10. As illustrated in this figure, the TWC never reached an idealized shape because the outside diameter crack half-length was always smaller than the inside diameter crack half-length after through-wall penetration. The inside diameter

16

crack length shows a slight change in the growth rate when the crack becomes a TWC at about 26 months, but it then returns to a more continuous crack growth rate. The outside diameter crack length shows that the crack moves from a transitioning TWC between 26 and 28 months to a shape close to an idealized TWC.
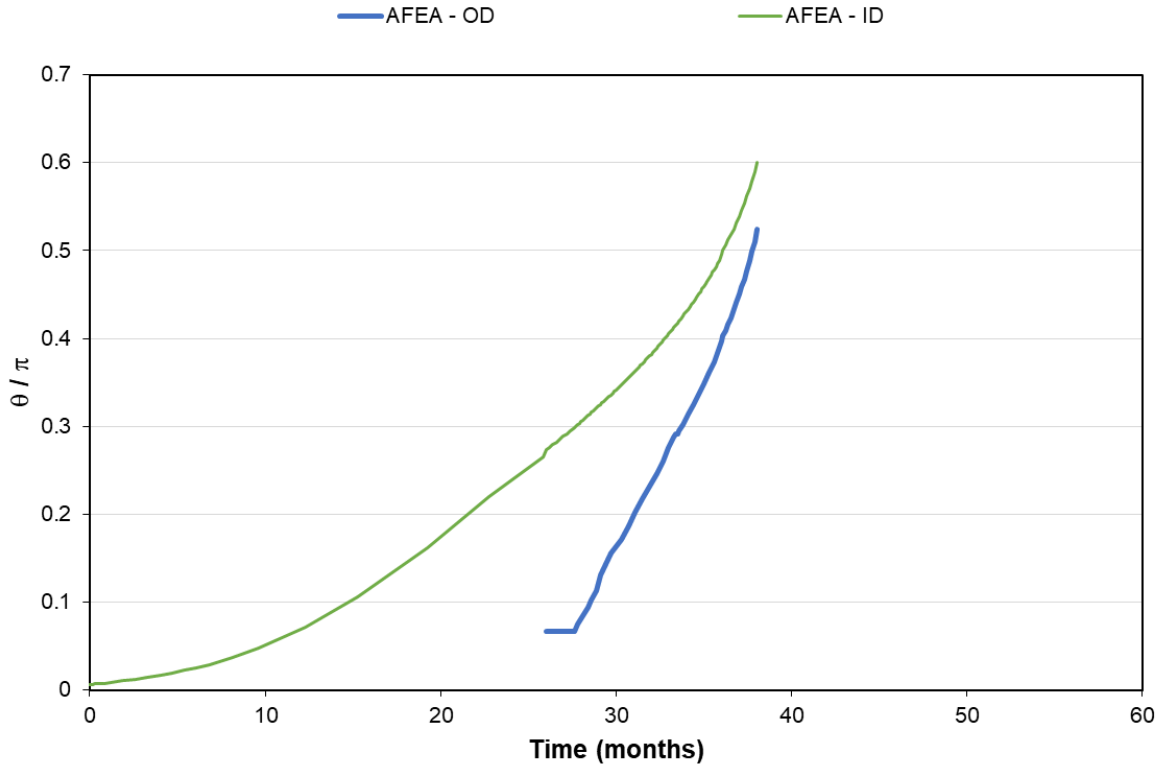
Figure 3-10   DP-01 inside and outside diameter crack lengths as a function of time (AFEA results)

The inside diameter crack length predicted by AFEA is expressed as a normalized angle around the circumference. Comparisons with all the PFM code predictions are shown in Figure 3-11 and only with the xLPR code in Figure 3-12. When the crack is a surface crack, the length on the inside diameter compares well with most of the PFM codes. However, when the crack penetrates through-wall, differences in the inside diameter crack length predictions begin to emerge. Several of the PFM codes, including xLPR, show a short but significant decline in the crack growth rate along the inside diameter, while several other PFM codes show a slight or even negligible change in slope. The xLPR code uses its crack transition model to apply correction factors to the SIFs and CODs until the TWC reaches an idealized shape. Most of the other PFM codes use a similar approach. The transition logic used in these codes has not previously been compared to natural crack growth methods such as AFEA, and the change in slope of the curves for most of the codes in Figure 3-11 does not appear to follow natural crack growth behavior. Indeed, the AFEA solutions show no change in slope. The final crack length was similar among all the PFM codes; however, the amount of time to reach the final crack length varied greatly.

Figure 3-11 **DP-01 AFEA inside diameter crack length compared to PFM code calculations**
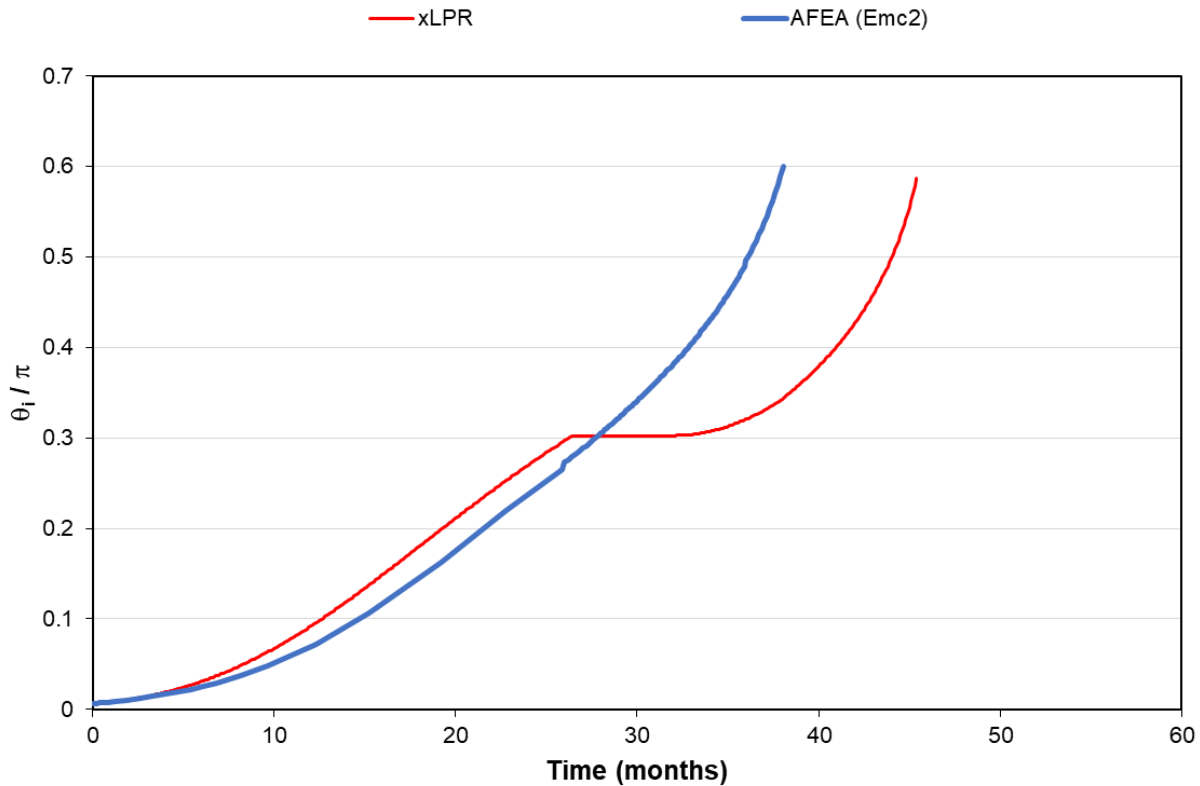
Figure 3-12   DP-01 AFEA inside diameter crack length compared to xLPR code calculations

Figure 3-13 shows a comparison of the outside diameter crack half-length angle, θ_o, predications from the PFM codes and AFEA. The AFEA-calculated crack growth is faster than many of the PFM codes, including xLPR, and seems to match the NURBIT code results most closely. Figure 3-14 specifically compares the AFEA and xLPR code predictions and highlights the faster crack growth on the outside diameter from the AFEA calculations.

The AFEA-calculated faster crack growth on the outside diameter, in conjunction with the faster crack growth on the inside diameter when the crack becomes through-wall, led to crack instability sooner than most of the PFM codes predicted. The differences in the crack growth rates may be related to the inclusion of crack transition models in most of the PFM codes, because the point of through-wall penetration is when differences in the predictions begin to emerge. The crack transition model in the xLPR code was developed based on analytical assumptions and could be improved using AFEA or additional testing data. Such improvements could lead to results closer to the AFEA predictions.
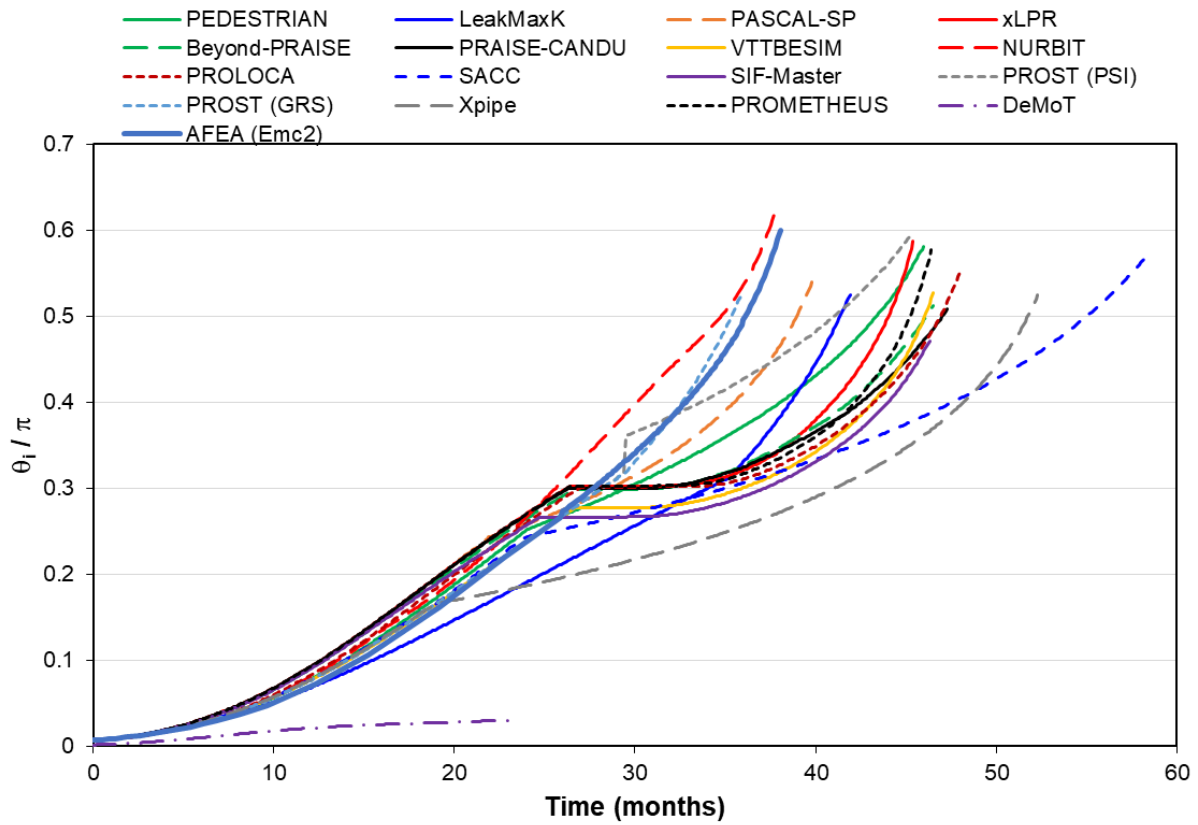
Figure 3-13   DP-01 AFEA outside diameter crack length compared to PFM code calculations
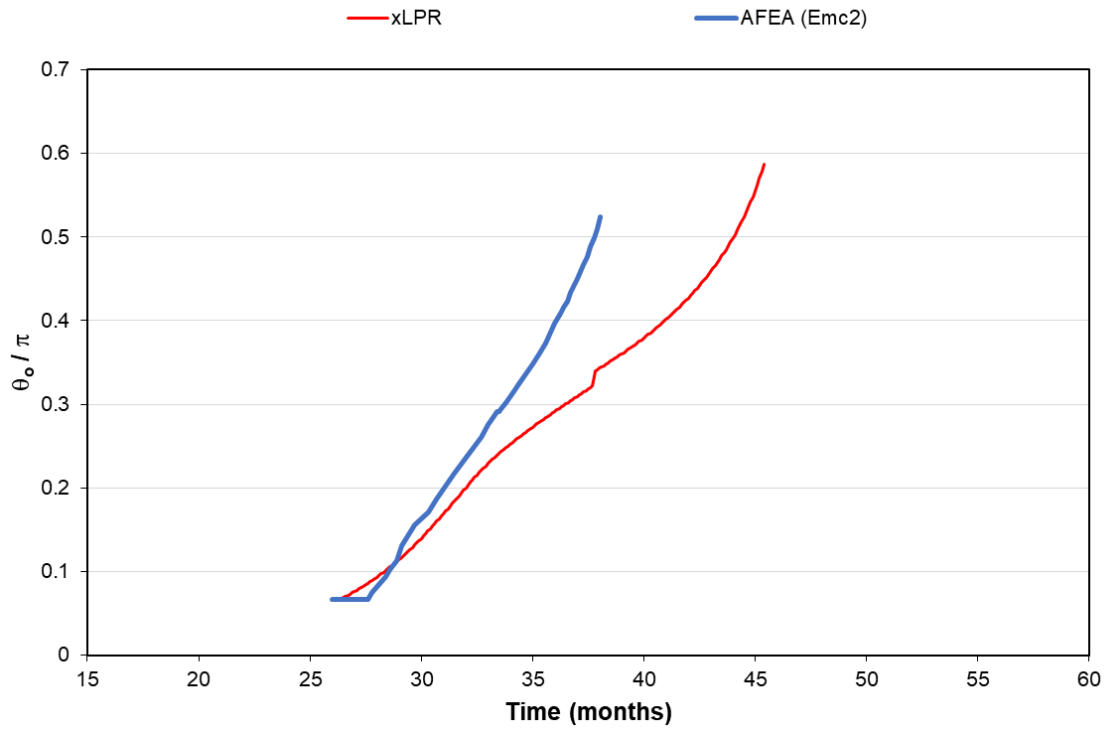
Figure 3-14   DP-01 AFEA outside diameter crack length compared to xLPR code calculations

3.2.2   DP-02 Crack Length Comparisons

The inside and outside diameter normalized crack half-lengths for DP-02 as determined by AFEA are shown in Figure 3-15.
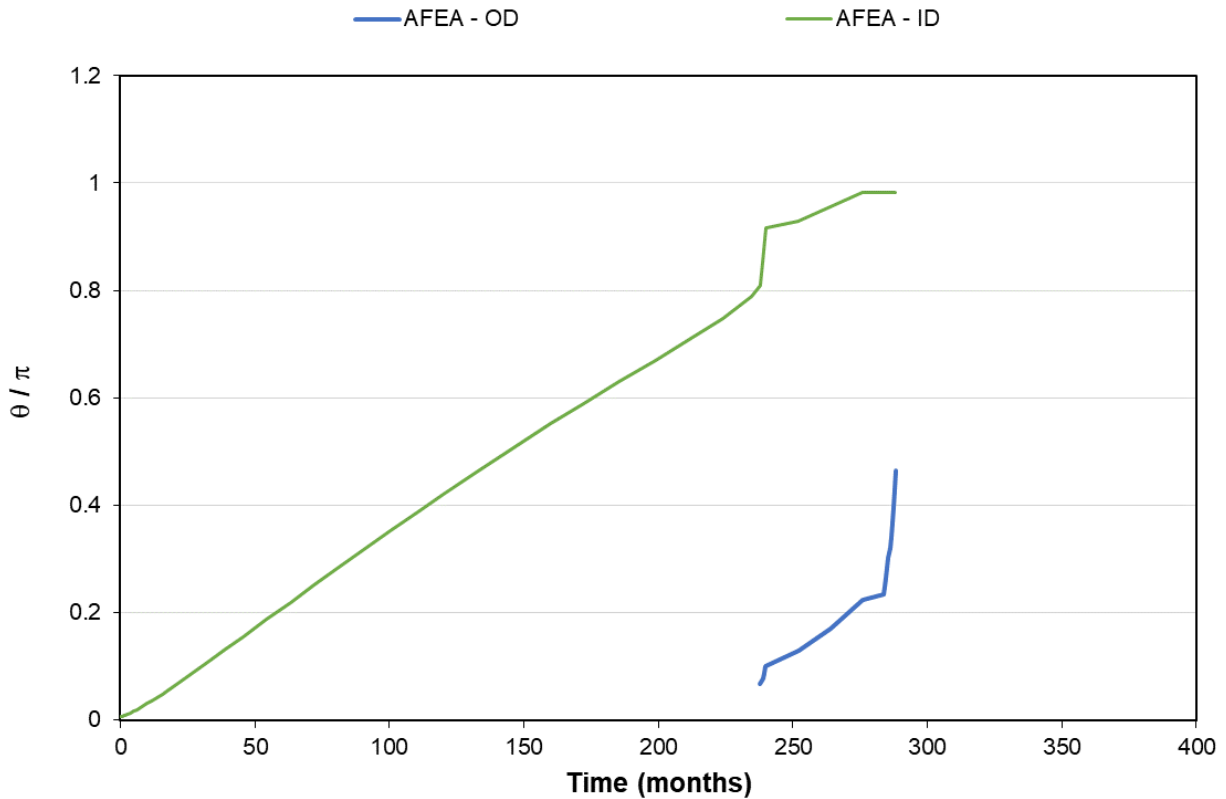
Figure 3-15   DP-02 inside and outside diameter crack lengths (AFEA results)

The AFEA-predicted inside diameter crack half-length angle, θ_i is compared to the predictions from all the PFM codes in Figure 3-16 and only to the xLPR code in Figure 3-19. There is good agreement among the PFM code and AFEA predictions for the inside diameter crack length over time, although AFEA predicted longer inside diameter crack lengths than all the other PFM codes except NURBIT. In fact, only NURBIT and AFEA predicted that the crack would grow all the way around the inside circumference before instability occurred.
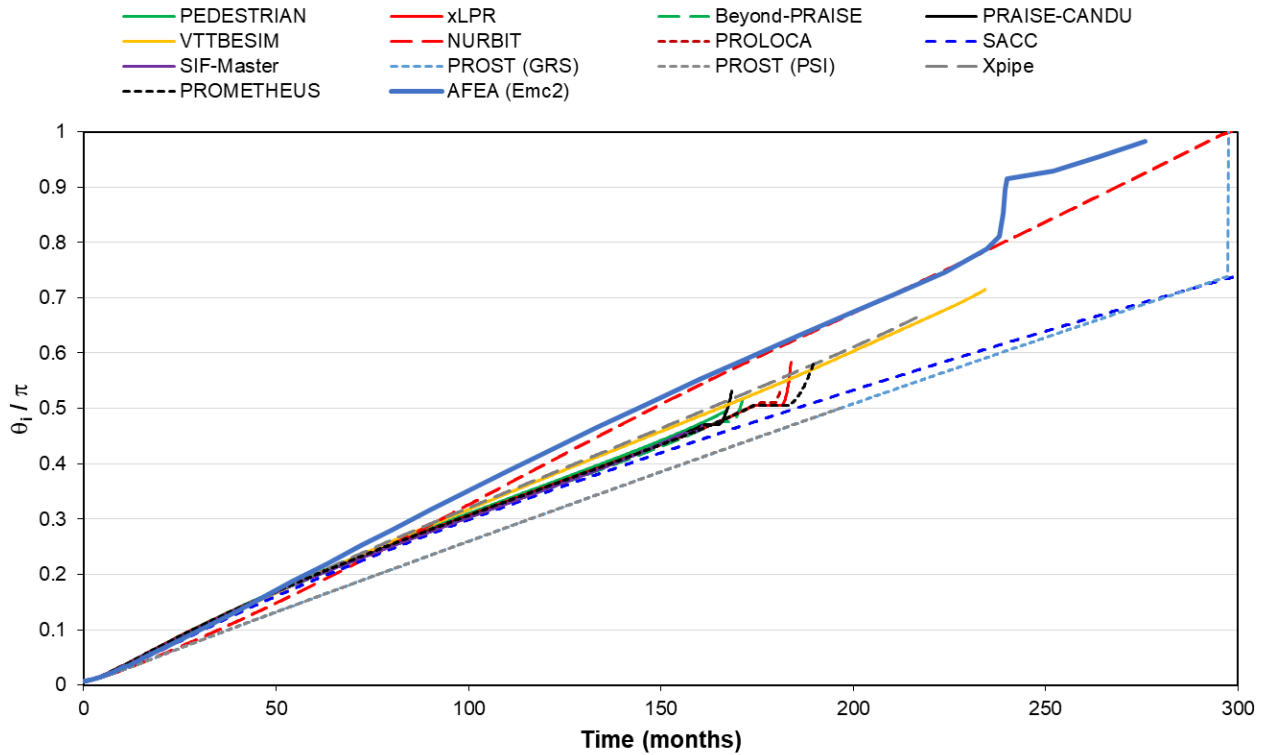
Figure 3-16   DP-02 AFEA inside diameter crack length compared to PFM code calculations

The AFEA predictions show that, when the crack grows into the compressive WRS field, growth in the depth direction slows considerably (as in Figure 3-9), and growth in the surface direction continues to grow quickly (as in Figure 3-15). In fact, the AFEA results show that the crack does not grow appreciably in the depth direction until it is about 300 degrees around the inside circumference. The AFEA results are shown in detail the sequence of mesh plots in Figure 3-17.
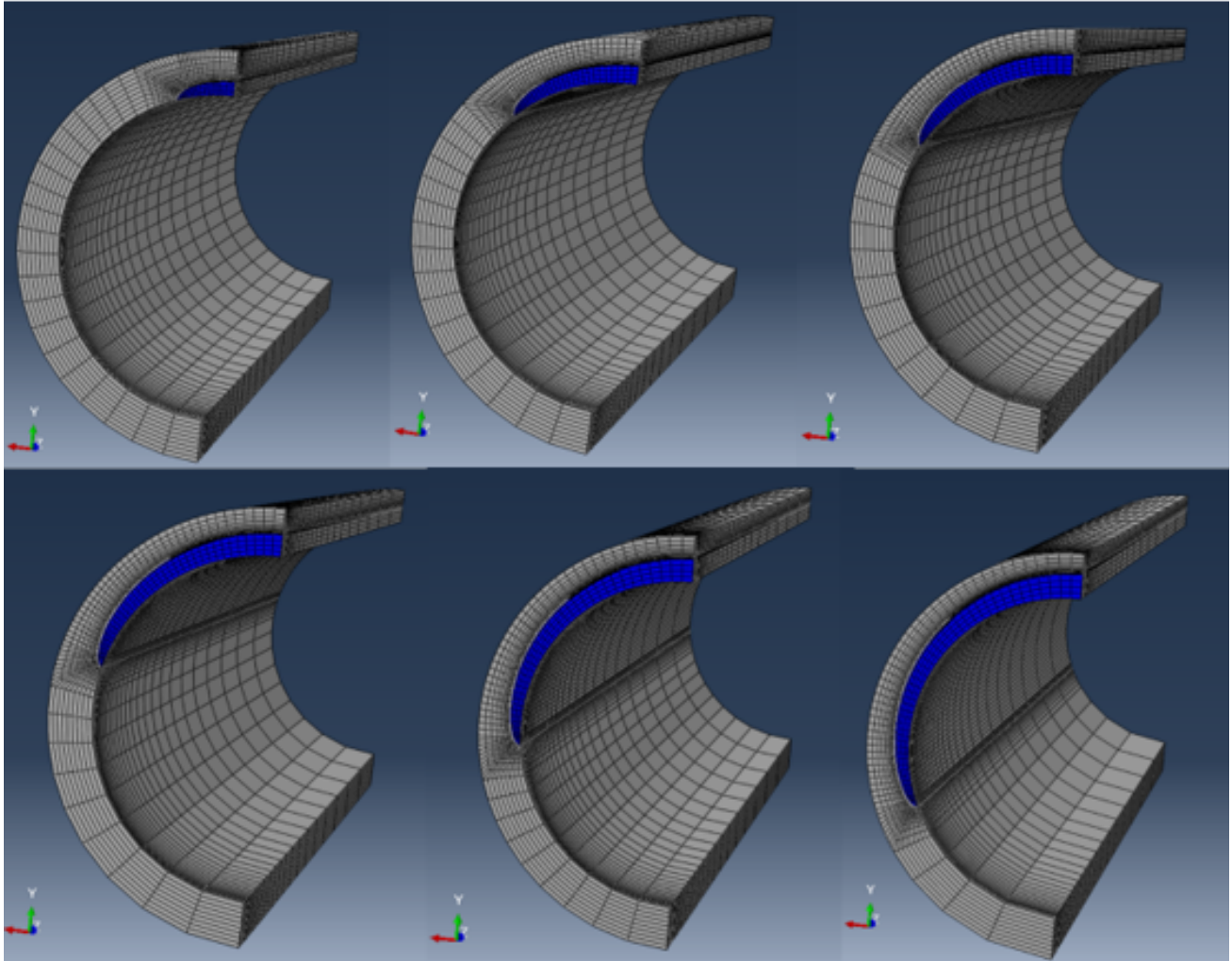
Figure 3-17   DP-02 sequence of crack growth through the compressive stress region as determined by AFEA

As Figure 3-17 shows, crack growth in the depth direction slows considerably while the crack continues to grow around the inside surface of the pipe, from about 10 to 70 percent of the circumference. Although crack growth slows in the depth direction, it does not stall. Once the crack grows through the compressive WRS region, it becomes a TWC when the length along the inside diameter is about 80 percent of the circumference, as shown in Figure 3-18.
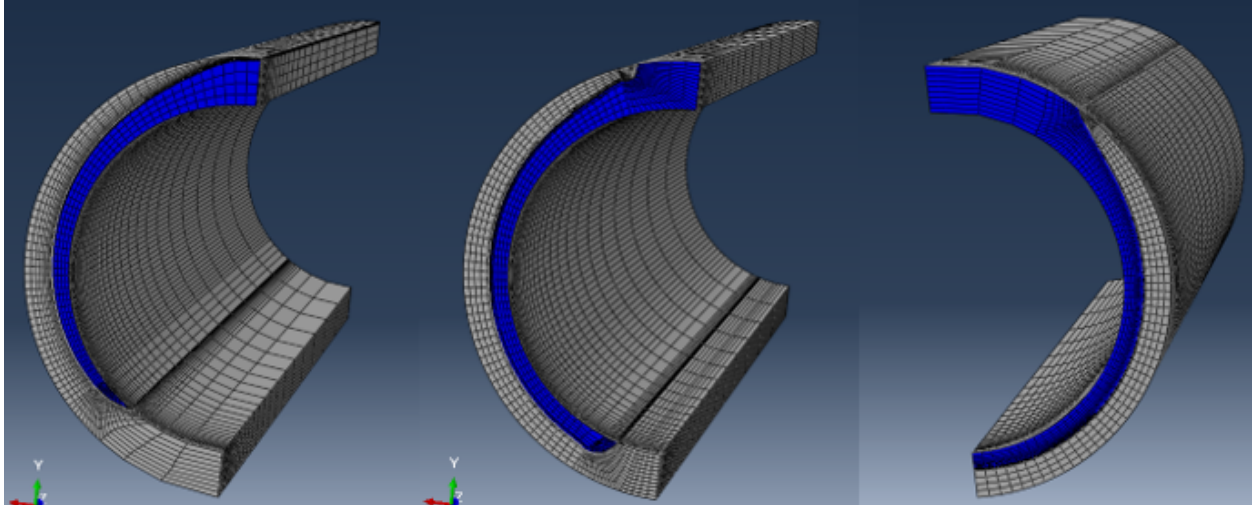
Figure 3-18   DP-02 sequence of crack growth from TWC to 360-degree inside surface crack

Once the crack becomes through-wall, it continues to grow around the inside surface until it reaches 360 degrees and becomes a complex crack. During this time, the crack also continues to grow on the outside surface, although at a slower rate than estimated by the xLPR code. The situation where the inside diameter crack length is very long relative to the outside diameter crack length increases the likelihood that failure may occur before the crack is detected, including when the surface crack grows the full 360 degrees around the inside circumference before becoming a TWC.

When a crack grows into a considerable compressive WRS field, such as in DP-02, it is possible that the inside diameter crack length could become 360 degrees before growing faster in the depth direction. This type of crack has been observed in service at Duane Arnold Energy Center as described in NUREG-0531, "Investigation and Evaluation of Stress-Corrosion Cracking in Piping of Light Water Reactor Plants," issued February 1979 [5], and represents a potential for break-before-leak. Further study of this phenomena would be useful because the xLPR code can currently only grow the crack at the depth and surface points, which can result in non-conservative results for some highly compressive, mid-thickness WRS fields.

The time to reach a TWC was around 160 months as calculated by the xLPR code and around 240 months as calculated by AFEA. As shown in Figure 3-9, the difference in time has a noticeable impact on the crack length once it leaks. Specifically, the xLPR code predicted an inside diameter crack length of 50 percent of the circumference while AFEA predicted a length of 80 percent.
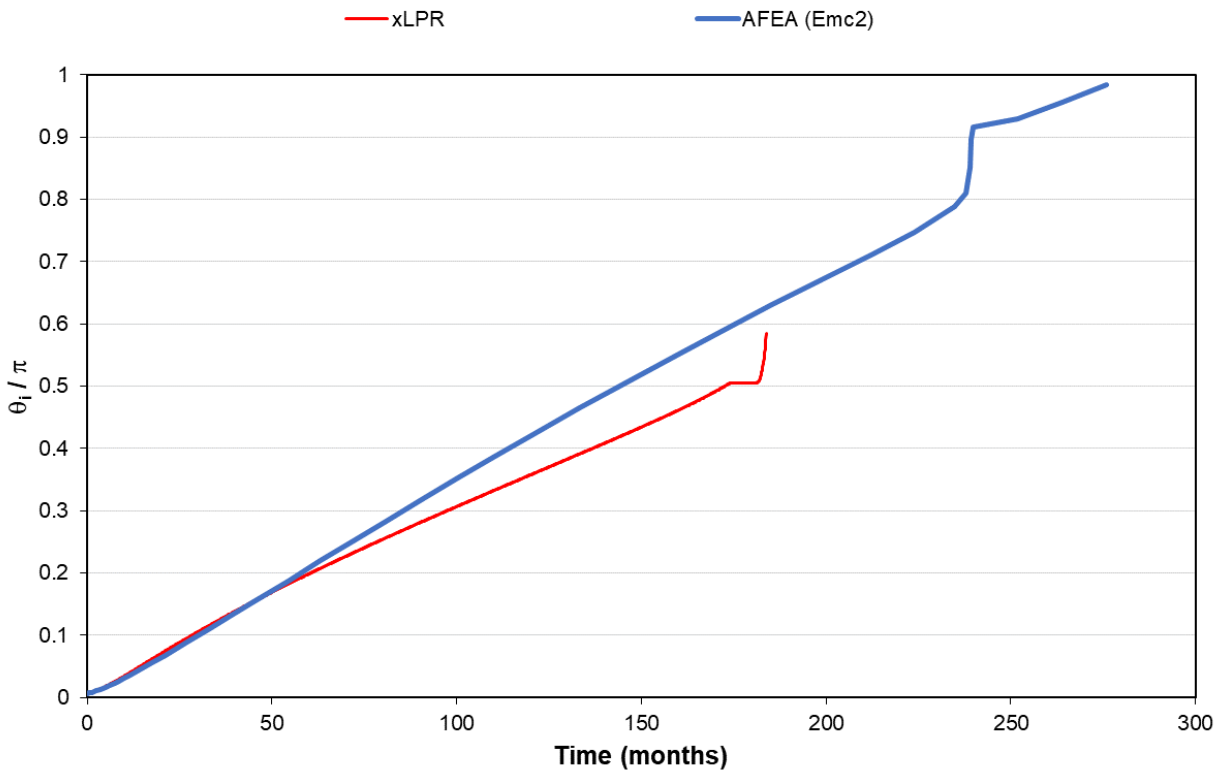
Figure 3-19   DP-02 AFEA inside diameter crack length compared to xLPR code calculations

A comparison of the outside diameter crack length predictions from all the PFM codes and AFEA is shown in Figure 3-20, and Figure 3-21 presents the comparison only between the AFEA and xLPR code results.
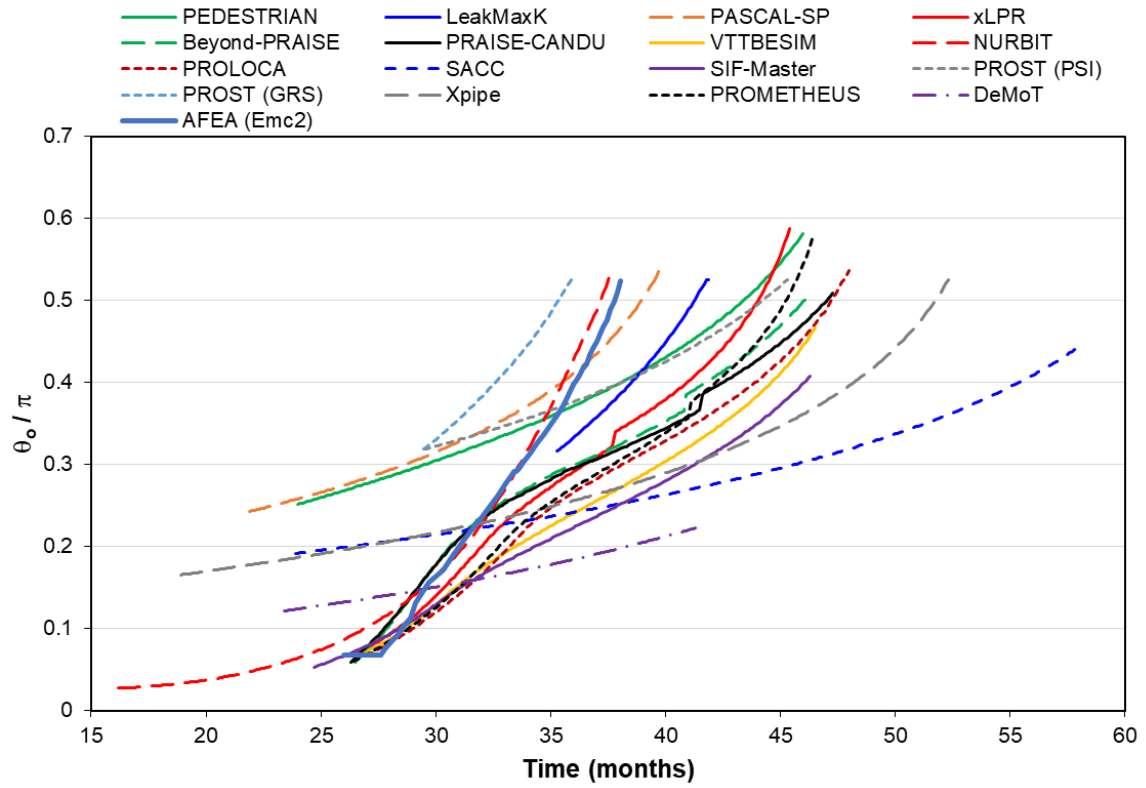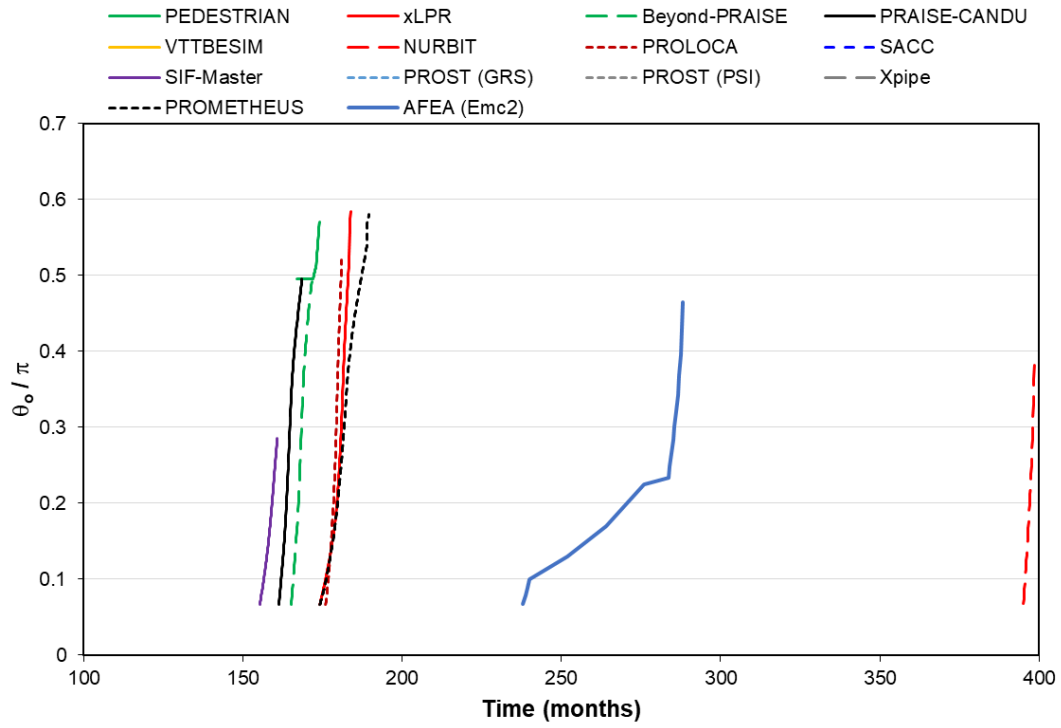
Figure 3-20   DP-02 AFEA outside diameter crack length compared to PFM code calculations
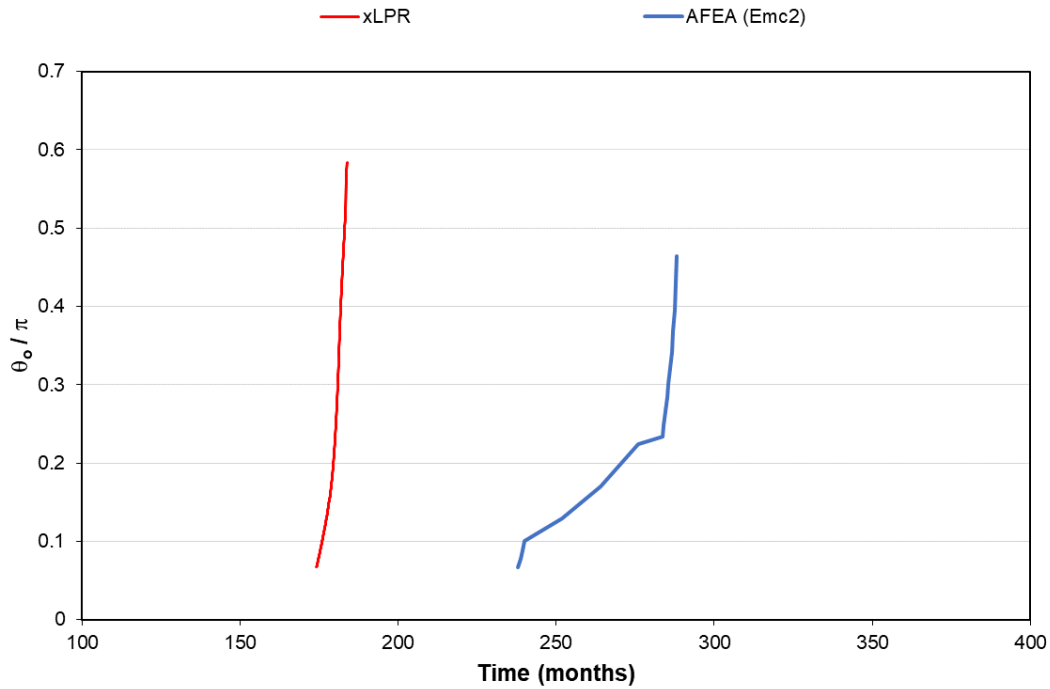
Figure 3-21   DP-02 AFEA outside diameter crack length compared to xLPR code calculations

Both Figure 3-20 and Figure 3-21 show that AFEA predictions differ from all the PFM code predictions. The PFM codes make similar predictions in the outside diameter crack growth rate, which include fast crack growth over a short period of time. In contrast, AFEA predicted a longer period of slower crack growth on the outside diameter before exhibiting the same fast crack growth as predicted by the PFM codes. The differences in the crack growth trends among AFEA and the PFM codes may also be related to the crack transition models; however, it is also influenced by the idealized crack shape assumption used by the PFM codes. Section 3.5.2 further discusses these differences.

3.3   SIF

The SIFs influence the crack growth rate through an equation with the following general form for stress corrosion cracking:

$$\frac{da}{dt} = \left[e^{-\frac{Q}{R}\left(\frac{1}{T}-\frac{1}{T_{ref}}\right)} \right] \alpha f K^{\beta} \qquad \text{Eq. 3}$$

In Equation 3:

da/dt is the crack growth rate for primary water stress corrosion cracking in m/s
Q is the activation energy, which was set to 130 kJ/mol
R is the universal gas constant, 8.314 x 10^{-3} kJ/mol-K
T is the operating temperature, which was set to 320 °C (593.15 K)

28

T_{ref} is the reference temperature, which was set to 598.15 K

α is the power law constant, which was set to 2.16 x 10^{-12} (m/s)/(MPa-m$^{0.5}$)$^{1.6}$

f is a factor used to introduce uncertainty, and it was not used in the deterministic comparisons by setting its value to 1.0

K is the SIF in MPa-m$^{0.5}$

β is the power law exponent, which was set to 1.6

The SIF depends on the shape, size, and location of the crack as well as the magnitude and distribution of the loads and WRS field. Therefore, the WRS can have a large impact on the SIF predictions. It is expected that the differences seen in the crack lengths discussed in Section 3.2 may be related to the SIFs predicted by AFEA and the PFM codes. Another important impact is the difference in crack shape evolution between natural (in AFEA) and assumed elliptical (in the PFM codes) crack growth. Although the AFEA procedure determines the SIFs at every node along the crack front, the PFM codes generally only determine the SIFs at one of the crack tips and at the deepest point through the thickness for a surface crack. Therefore, the comparisons of the PFM code and AFEA predications only considered these two points.

It is important to understand how the calculation of the SIFs changes as the crack moves from a surface crack to a transitioning crack and then to an idealized TWC. For a surface crack, the SIF is calculated at the inside diameter crack tip, K_{I_b}, and at the center of the crack or deepest point through the thickness, K_{I_a}. For a TWC, the SIF is calculated at the inside diameter crack tip (also referred to in the benchmarking study as K_{I_b}) and at the outside diameter crack tip (also referred to in the benchmarking study as K_{I_a}). Most of the PFM codes assume an idealized TWC when calculating K_{I_a} and K_{I_b}. Several of the PFM codes, including xLPR, have crack transition models that calculate the SIFs between when the crack is a surface crack and when it becomes an idealized TWC. SIFs in the transition period are determined by applying a correction factor that has been calibrated using results from three-dimensional FEA for a limited range of crack length ratios based on the work of Shim [6]. Although three-dimensional FEA of non-idealized TWC shapes accounted for curvature of the crack front, complex crack fronts were not considered.

3.3.1 DP-01 SIF Comparisons

A comparison of the DP-01 K_{I_b} predictions from the PFM codes and AFEA is shown in Figure 3-22. Figure 3-23 compares only the AFEA and xLPR code predictions. These comparisons reveal two primary differences between the AFEA and PFM code predictions:

(1) While the crack is a surface crack, AFEA predicts lower SIFs than almost all the PFM codes and, except for DeMoT, the PFM codes show the same trend and similar SIF values. Most of the PFM codes show a sharp drop in the SIF values when the crack becomes a TWC followed by an increase as the crack continues to grow on the outside diameter surface. The sharp drop is due to the correction factors that are applied to the SIFs according to the crack transition models in the PFM codes.

(2)   The AFEA results do not show the sharp drop in the SIF values as the crack becomes a TWC at 25.85 months. Instead, the AFEA results show a slight increase. This result is because the AFEA procedure can model crack growth more realistically and without relying on the simplifications in the PFM code crack transition models. After transitioning to an idealized crack shape or close to it, the K_{I_b} values are nearly identical between the AFEA and xLPR code predictions.

Figure 3-22   DP-01 AFEA SIFs at the inside diameter crack tip compared to PFM code calculations

Figure 3-23   DP-01 AFEA SIFs at the inside diameter crack tip compared to xLPR code calculations

A comparison of the DP-01 K_{I_a} from the AFEA and PFM code predictions is shown in Figure 3-24. Figure 3-25 compares only the AFEA and xLPR code predictions. Both figures show the SIFs for up to three different crack shapes from the PFM codes (i.e., surface crack, transitioning crack, and an idealized TWC). AFEA can produce a TWC with a complex (i.e., non-idealized) shape. The K_{I_a} values for surface cracks up to approximately 26 months are nearly identical for all the PFM codes and AFEA predictions. These results are consistent with the similarities in the crack depth curves presented in Section 3.1.1. There are more differences in the K_{I_a} predictions when the crack becomes a TWC. Only AFEA predicts a continuously increasing SIF with some single point drops as the analysis converged. Except for LeakMaxK, the PFM codes all show a vertical jump in the SIF values as the crack becomes a TWC. These step increases are the result of the correction factors applied by the crack transition models, and they mark the start of the phase when the crack is transitioning. A few of the PFM codes (i.e., Xpipe, SACC, DeMoT, and PEDESTRAIN) then transition to a parabolic increase in the SIF values while the rest of the PFM codes show a transitioning section starting with a linear increase followed by parabolic behavior. This behavior corresponds to the phase when the crack is an idealized TWC. These differences led to the increased scatter in the outside diameter crack length predictions as shown in Figure 3-13.

31

Figure 3-24   DP-01 AFEA SIFs at the deepest point and outside diameter crack tip compared to PFM code calculations

Figure 3-25   DP-01 AFEA SIFs at the deepest point and outside diameter crack tip compared to xLPR code calculations

3.3.2   DP-02 SIF Comparisons

A comparison of the DP-02 K_{I_b} predictions from the PFM codes and AFEA is shown in Figure 3-26. Figure 3-27 compares only the AFEA and xLPR code predictions. As with DP-01, these figures show the SIF values for up to three different crack shapes from the PFM codes (i.e., surface crack, transitioning crack, and idealized TWC). The AFEA-predicted SIF values are relatively constant over the entire crack shape evolution. There is a slight change when the crack becomes a TWC and then the SIFs become negative when a 360-degree surface crack is reached. A few of the PFM codes also predict relatively constant SIF values, specifically NURBIT, VTTBESIM, Xpipe, SACC, and PROST. The other PFM codes show similar predictions while the crack is a surface crack up to about 170 months. These PFM codes then show a drop close to zero due to the applied correction factors from the crack transition models followed by dramatic increases over a short period of time as the crack becomes an idealized TWC.
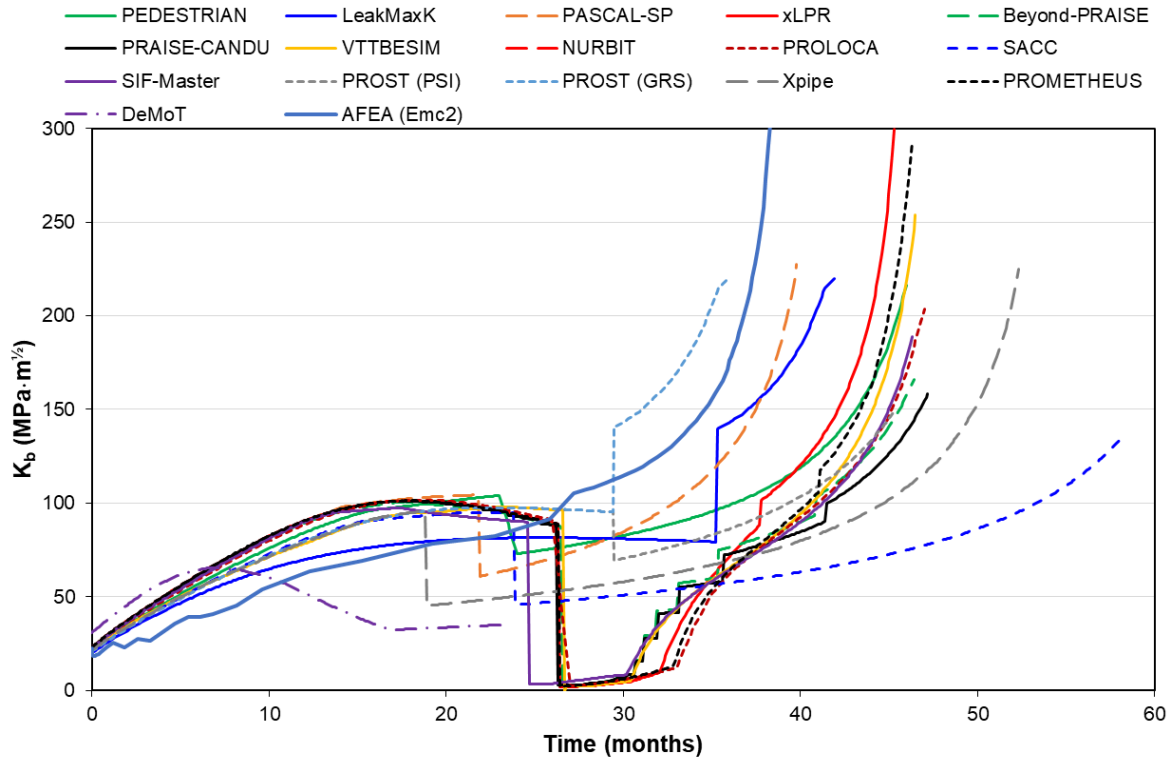
33
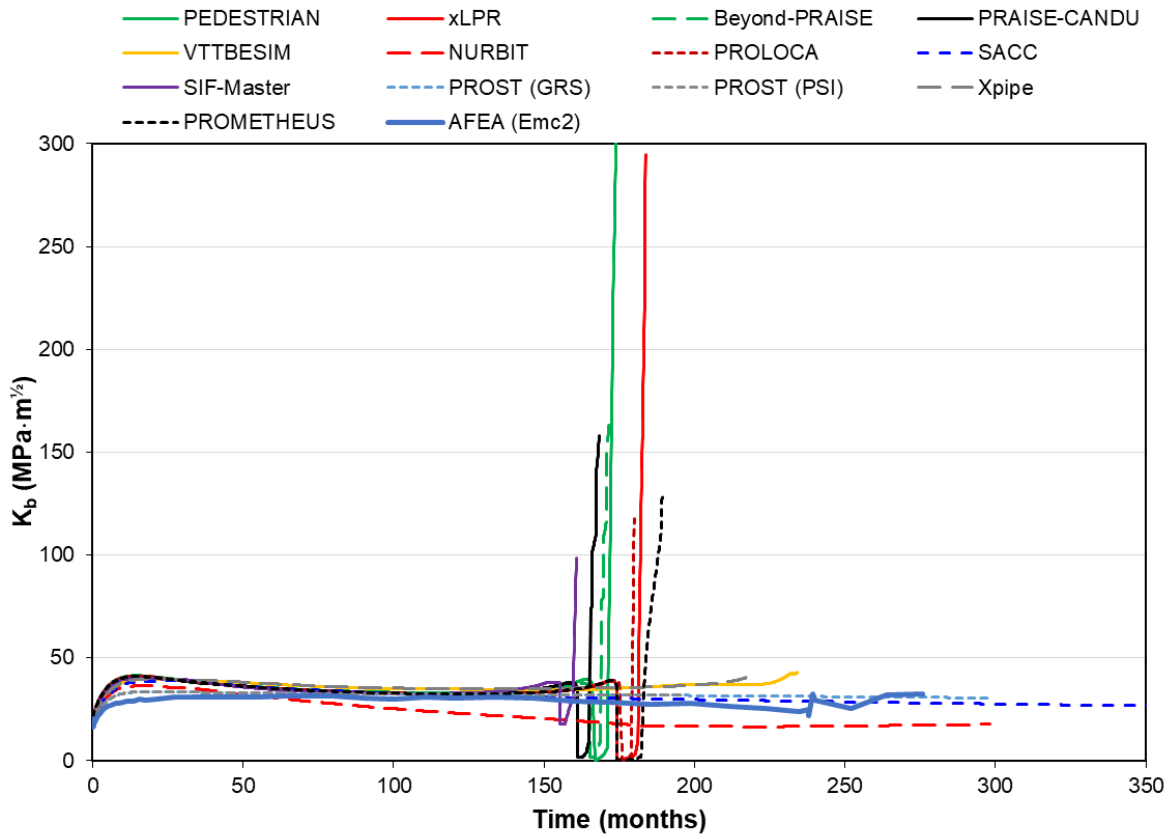
Figure 3-26   DP-02 AFEA SIFs at the inside diameter crack tip compared to PFM code calculations
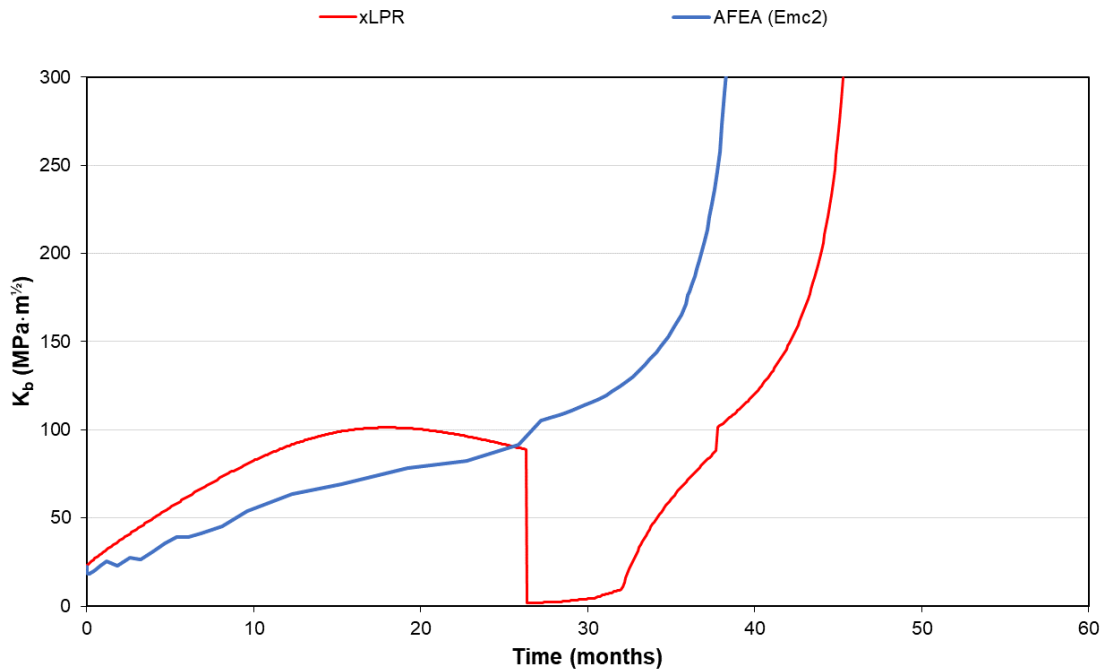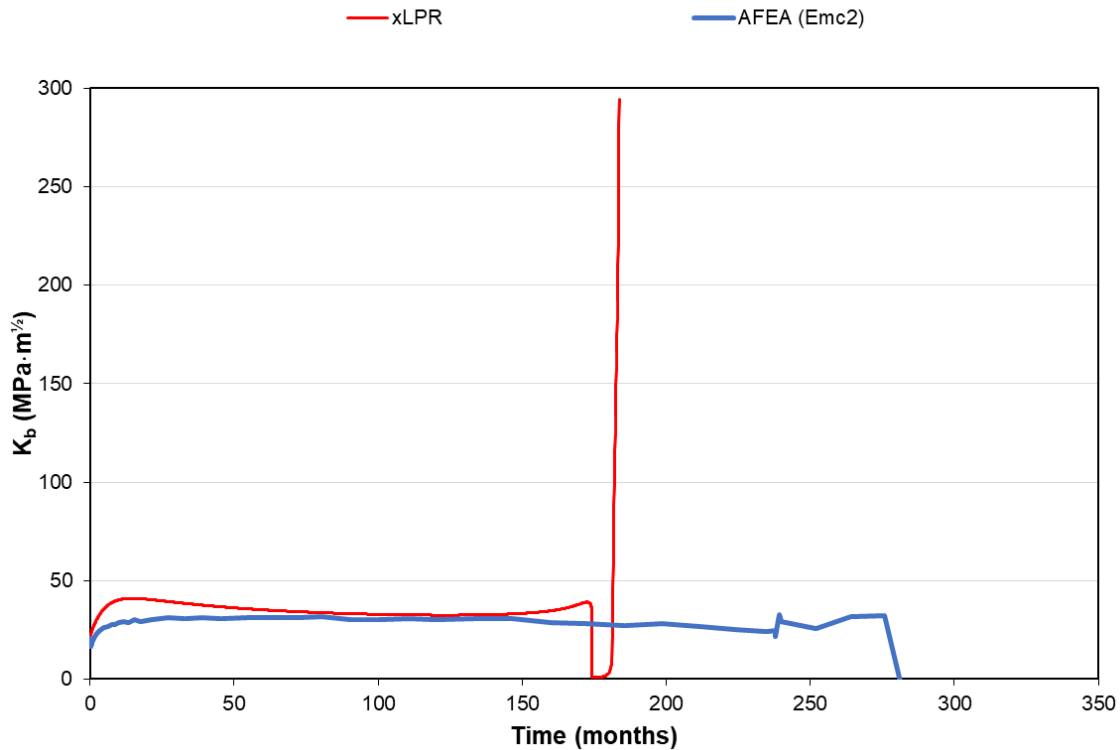
Figure 3-27   DP-02 AFEA SIFs at the inside diameter crack tip compared to xLPR code calculations

A comparison of the DP-02 K_{I_a} values from the AFEA and PFM code predictions is shown in Figure 3-28. Figure 3-29 compares only the AFEA and xLPR code predictions. The PFM codes and AFEA generally predict similar behavior. The primary difference is when the crack becomes a TWC. AFEA predicts a period of slowly increasing SIFs after a small drop as the crack penetrates through-wall, and this behavior is different from all the PFM code predictions. As discussed in Section 3.2.2, when comparing the outside diameter crack length predictions, the difference is likely due to the crack transition models and idealized crack shape assumptions used by the PFM codes.
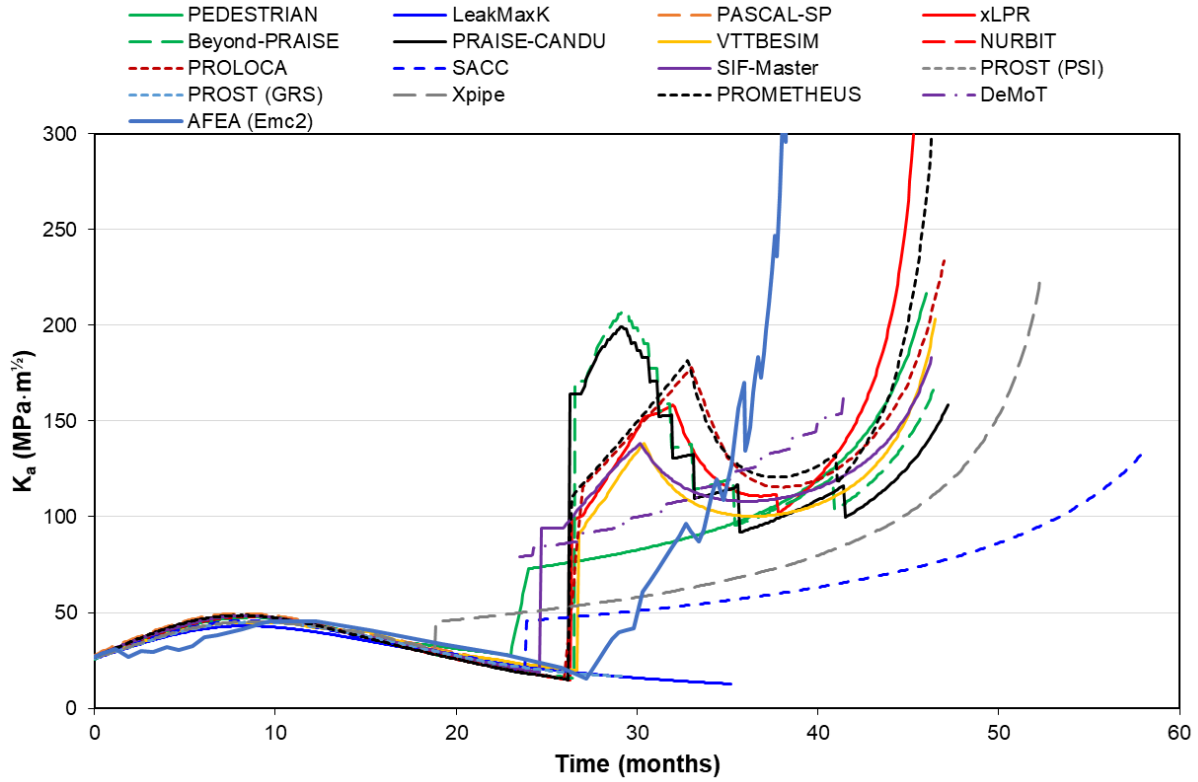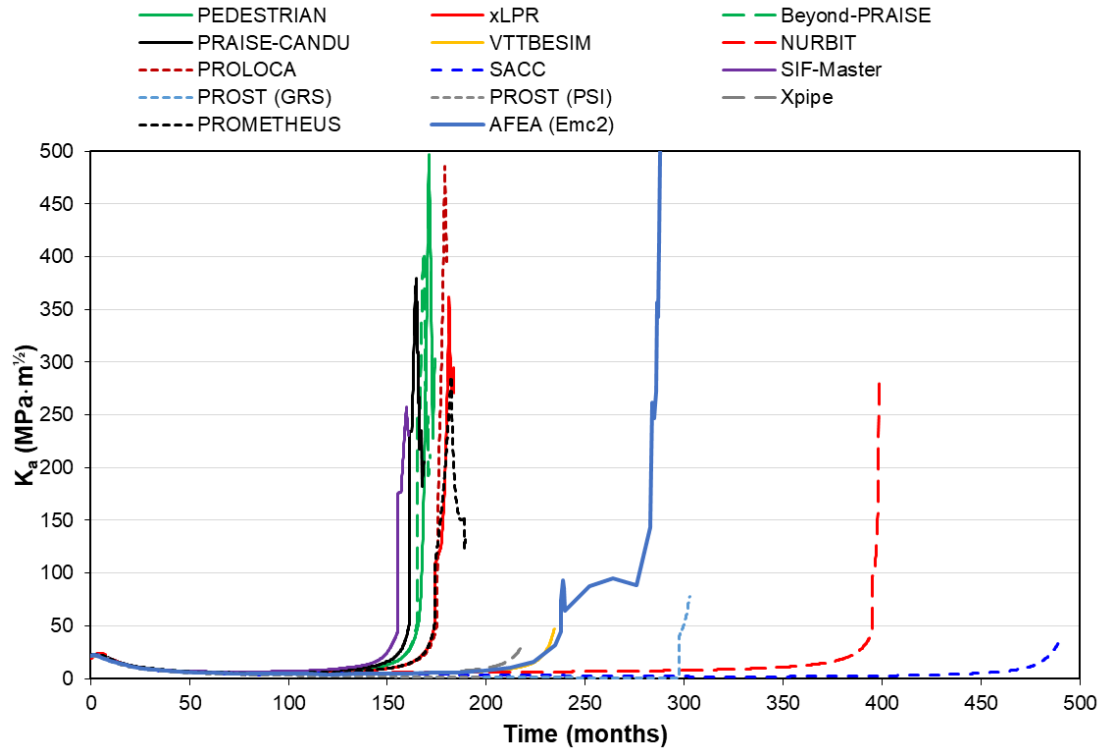
Figure 3-28   DP-02 AFEA SIFs at the deepest point or outside diameter crack tip compared to the PFM code calculations
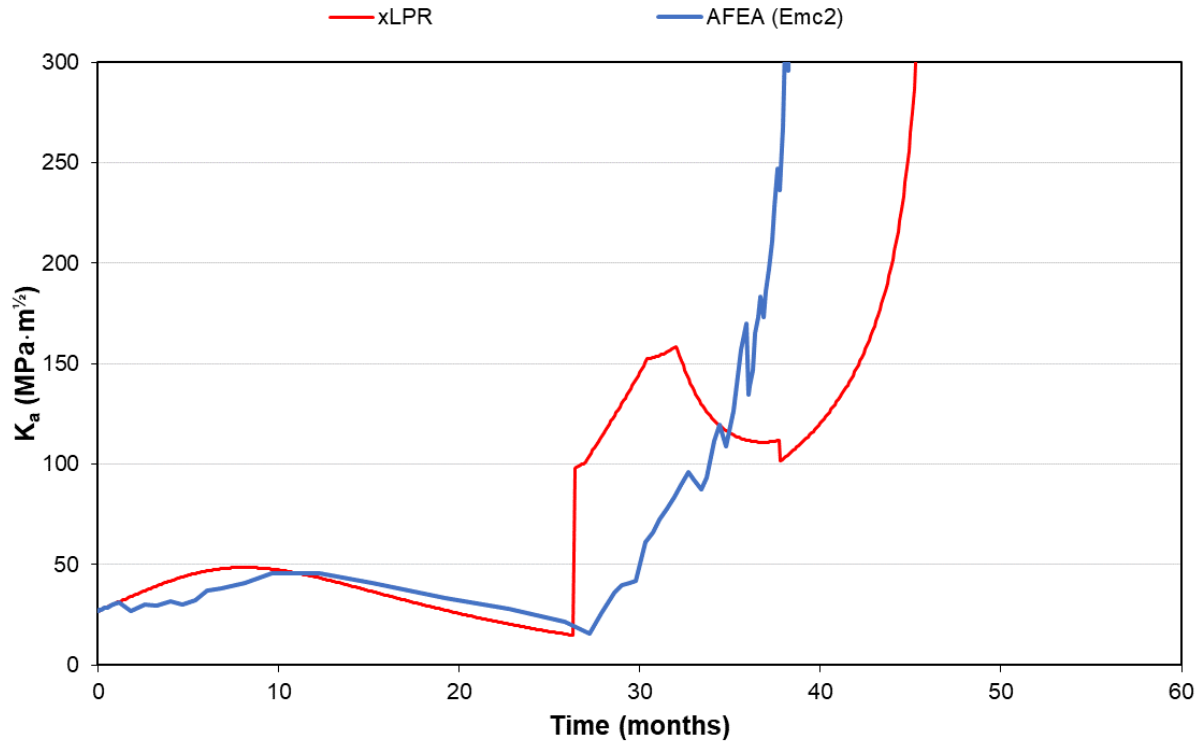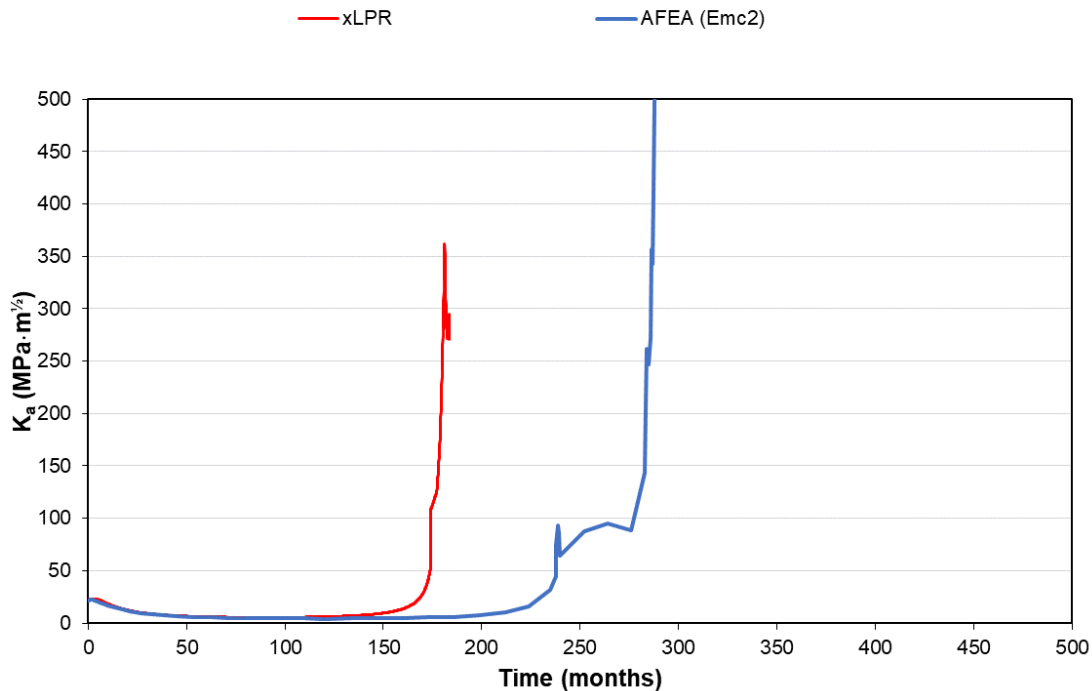
Figure 3-29   DP-02 AFEA SIFs at the deepest point or outside diameter crack tip compared to xLPR code calculations

3.4   COD

The COD is an important parameter in determining the leak rate of a given crack, and the leak rate is key in determining the LBB behavior of a piping component. Accordingly, CODs and the impact of the WRS on the CODs were examined.

3.4.1   DP-01 COD Comparisons

A comparison of the DP-01 inside diameter COD predictions from the PFM codes and AFEA is shown in Figure 3-30, where δ_i represents the COD at the inside surface, and c_i represents the absolute crack half-length at the inside surface. Figure 3-31 compares only the AFEA and xLPR code predictions. The CODs were only compared for TWCs. When the crack becomes a TWC, the PFM codes, including xLPR, no longer include crack face pressure; however, the AFEA included crack face pressure throughout crack growth, including after the crack becomes through-wall. The inclusion of crack face pressure is why AFEA predicted larger COD values at earlier times compared to the PFM codes.

37

Figure 3-30   DP-01 AFEA inside diameter CODs compared to PFM code calculations
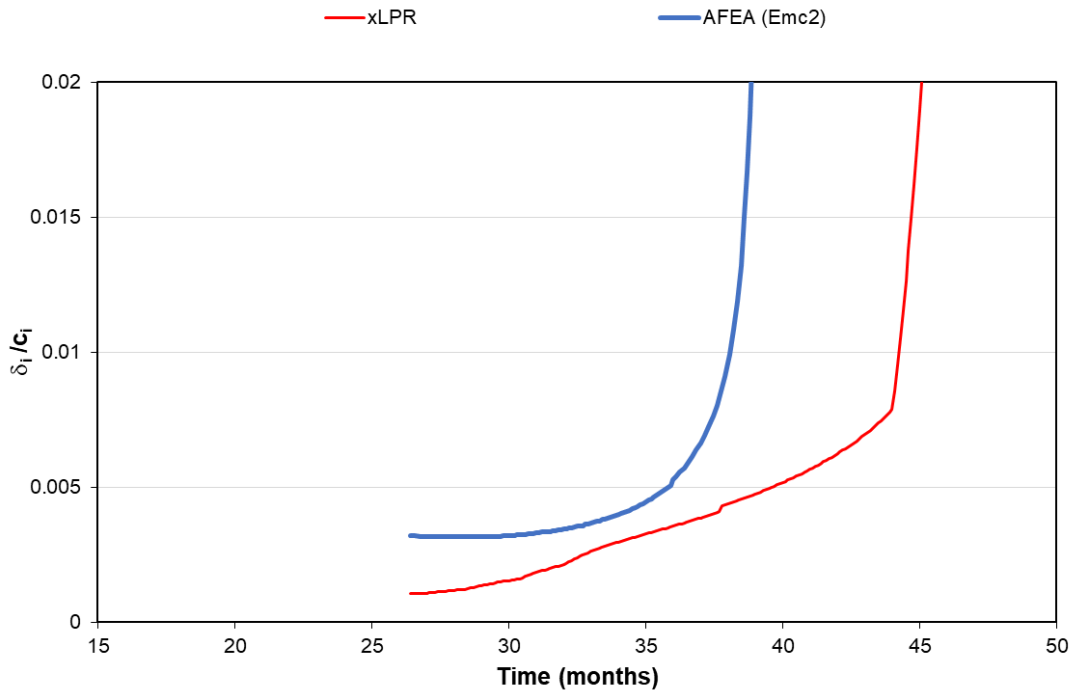
Figure 3-31   DP-01 AFEA inside diameter CODs compared to xLPR code calculations

A comparison of the DP-01 outside diameter COD predictions from the PFM codes and AFEA is shown in Figure 3-32, where δ_o represents the COD at the outside surface, and c_o represents the absolute crack half-length at the outside surface. Figure 3-33 compares only the AFEA and xLPR code predictions. The COD predictions are consistent with the outside diameter crack length predictions shown in Figure 3-14. Like the inside diameter COD predictions, the AFEA-predicted CODs on the outside diameter are larger at earlier times due to the inclusion of crack face pressure when the crack is a TWC. The PFM codes only include crack face pressure when the crack is a surface crack.

Figure 3-32   DP-01 AFEA outside diameter CODs compared to PFM code calculations
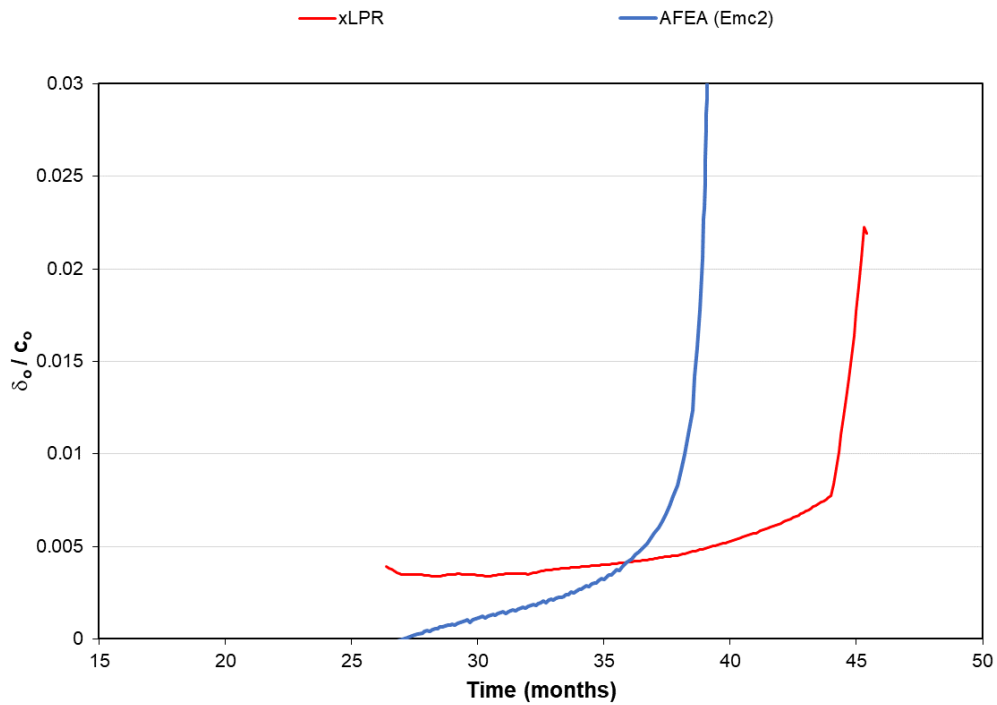
Figure 3-33   DP-01 AFEA outside diameter CODs compared to xLPR code calculations

3.4.2   DP-02 COD Comparisons

A comparison of the DP-02 inside diameter COD predictions from the PFM codes and AFEA is shown in Figure 3-34. Figure 3-35 compares only the AFEA and xLPR code predictions. The COD comparisons were again made only for TWCs. These predictions are consistent with the inside diameter crack length predictions shown in Figure 3-16 and Figure 3-19.
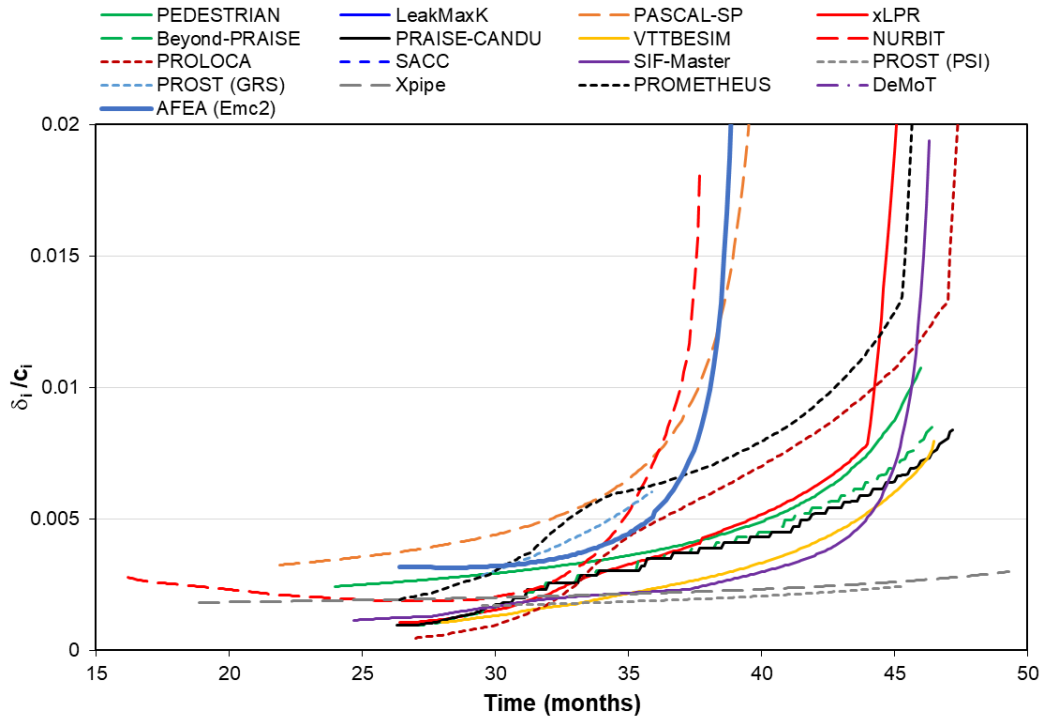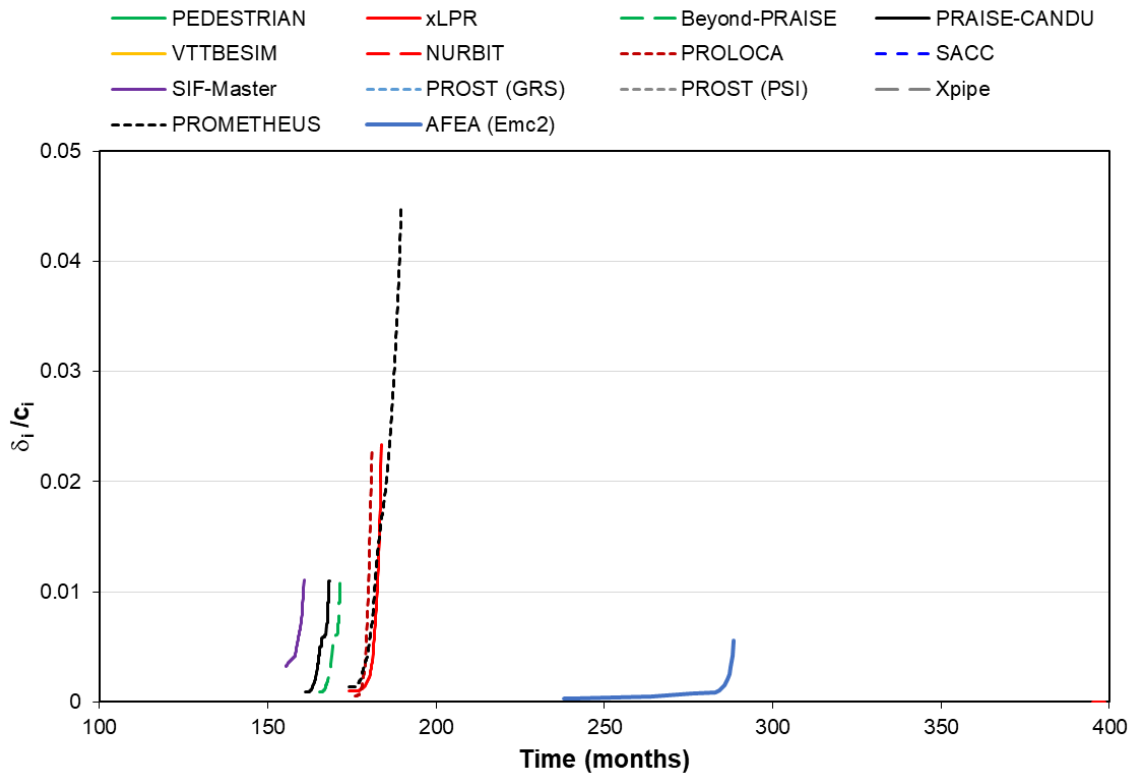
Figure 3-34 DP-02 AFEA inside diameter CODs compared to PFM code calculations
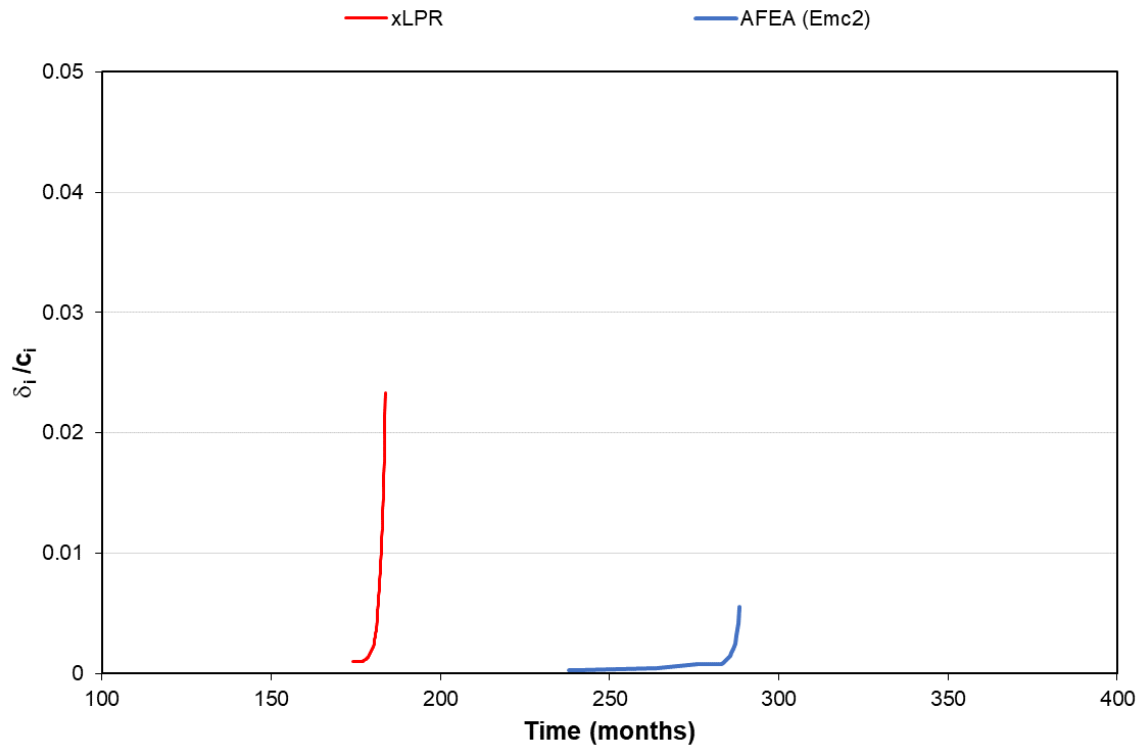
Figure 3-35   DP-02 AFEA inside diameter CODs compared to xLPR code calculations

A comparison of the DP-02 outside diameter COD predictions from the PFM codes and AFEA is shown in Figure 3-36. Figure 3-37 compares only the AFEA and xLPR code predictions. These predictions are consistent with the outside diameter crack length predictions shown in Figure 3-20 and Figure 3-21. Several curves show what appears to be a decrease in the COD values because they were normalized by the crack length on the outside diameter. The ratio of the COD to the crack length decreases because the outside diameter crack length is growing more quickly than the COD is increasing while the crack is transitioning to an idealized TWC. The COD is discussed further regarding its impact on the leak rate in Section 3.5.
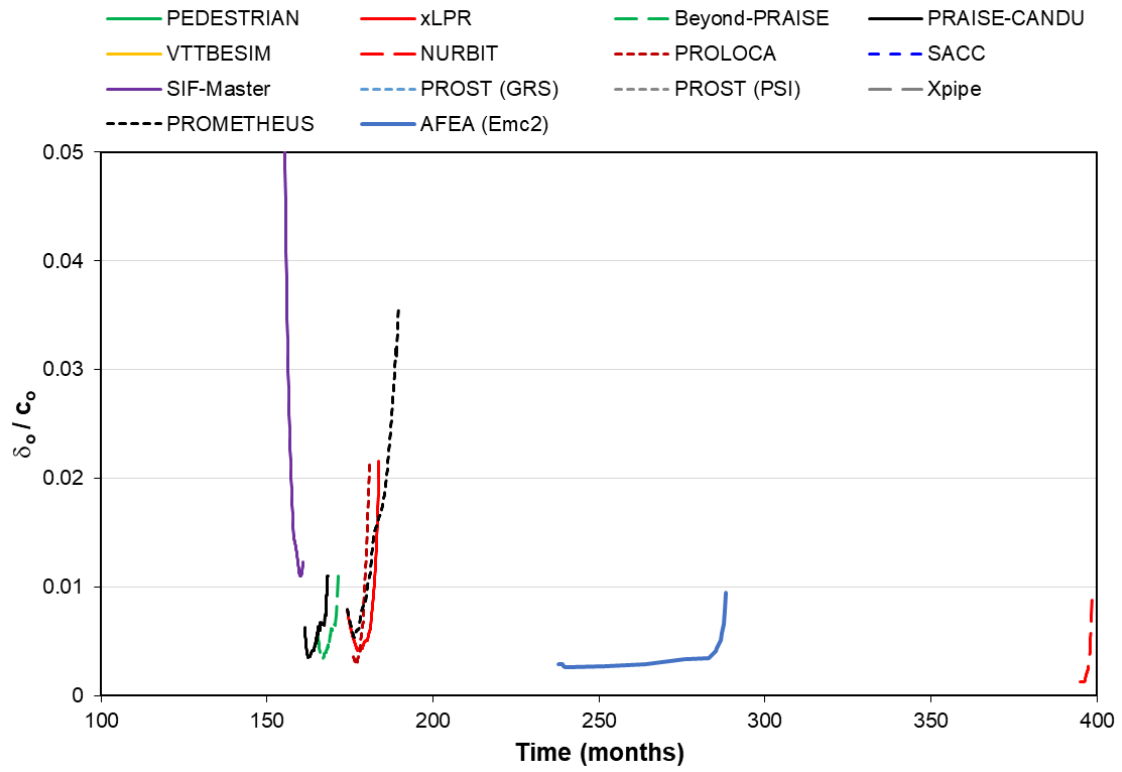
Figure 3-36   DP-02 AFEA outside diameter CODs compared to PFM code calculations

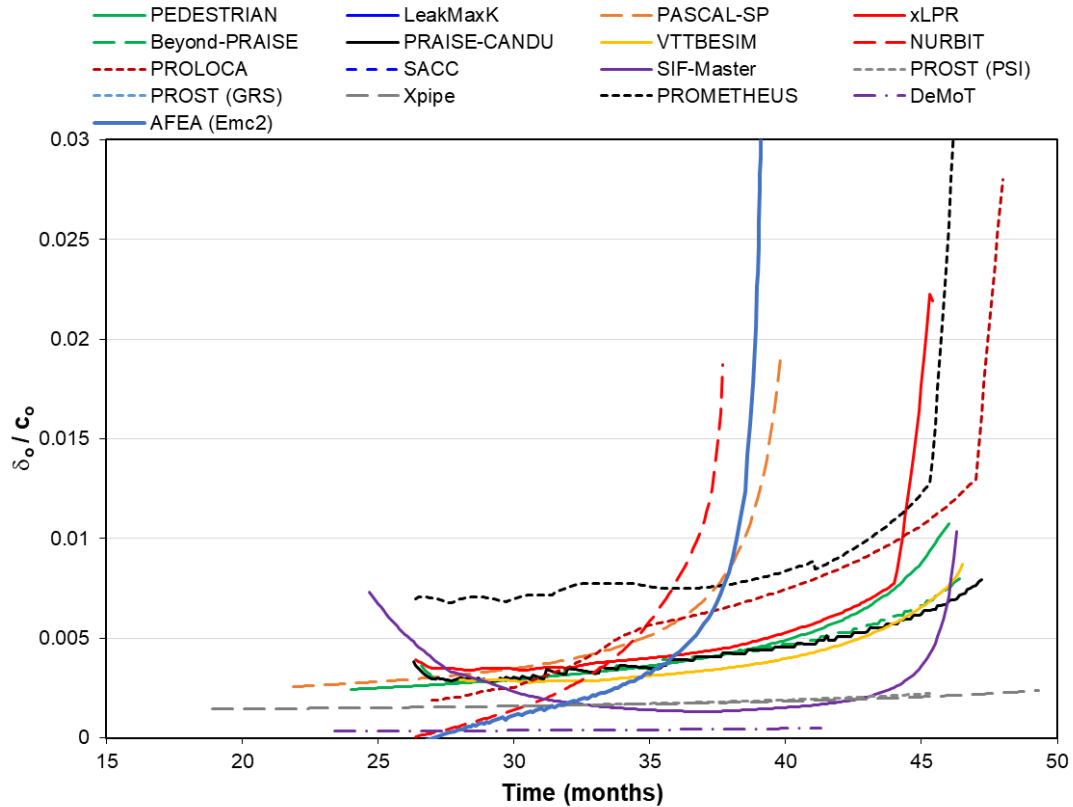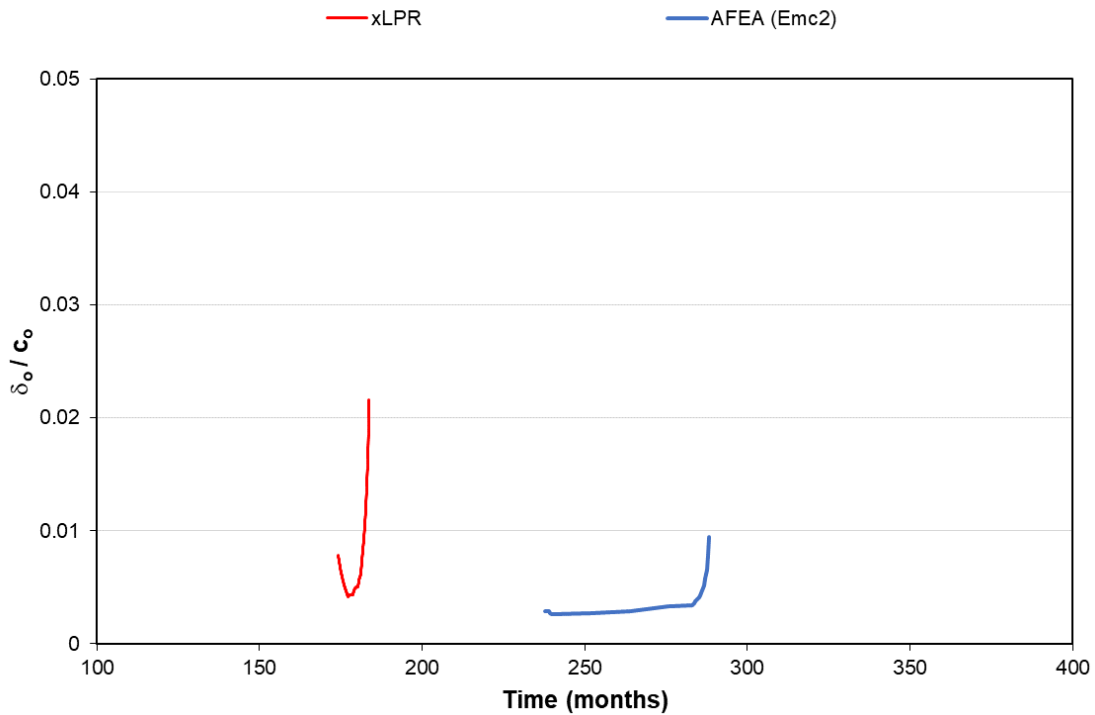**Figure 3-37   DP-02 AFEA outside diameter CODs compared to xLPR code calculations**

The DP-02 COD predictions on both the inside and outside diameters differ significantly from the DP-01 COD predictions from both the PFM codes and AFEA. Since the only difference between DP-01 and DP-02 is the WRS profile, it is logical to assume that the WRS has a significant impact on the predicted COD. Such an impact was also observed in a separate study presented in an NRC Technical Letter Report titled, "Estimation Scheme for Weld Residual Stress Effect on Crack Opening Displacements," issued in 2021 [7]. In comparing the DP-01 and DP-02 COD predictions from AFEA, it is apparent that the WRS effect can be significant. However, the AFEA results reveal that the crack shape is also a factor.

The AFEA-predicted crack shape for DP-01 before through-wall penetration is close to elliptical as shown in Figure 3-40, which was like the PFM code predictions. Therefore, as the crack grows after through-wall penetration, it maintains a shape closer to an idealized TWC. For this reason, the PFM code and AFEA predictions had better agreement for DP-01. However, the AFEA-predicted crack shape for DP-02 was complex as shown in Figure 3-43, and the complex crack shape is maintained when the crack becomes through-wall. Conversely, the PFM codes assume an idealized crack shape. As a result, the crack in the AFEA simulation has more time to grow through the thickness, which leads to a smaller exit opening of the TWC on the outside diameter surface and a more slowly increasing COD as compared to the PFM code predictions.

3.5   Leak Rate

The leak rate is important in determining the LBB behavior of a piping component because it determines whether a crack with a given leak rate can be detected and mitigated before a rupture occurs. However, the leak rate calculations have much uncertainty, not only because of the complexity of the fluid flow, but also because of the roughness and curviness of the crack, which are characterized by the crack morphology. The AFEA procedure itself does not determine the leak rate; however, the crack size calculated by the AFEA procedure at a particular time step can be used as an input to the LEAPOR code. Specifically, the AFEA-generated crack lengths and CODs on the inside and outside diameters along with other parameters specified for the benchmark problem were used as inputs to the LEAPOR code to calculate leak rates. The LEAPOR code can accept different crack sizes on the inside and outside diameters as inputs, although it uses an average of those values to calculate the leak rate. Many of the PFM codes use the same basic Henry-Fauske thermohydraulic model [8] [9] [10] that is used in LEAPOR. However, there may be differences among the PFM codes in how the crack morphology, different inside and outside diameter crack sizes, and uncertainties are handled. Even small changes in the inputs can lead to relatively large differences in the calculated leak rates. Accordingly, the leak rates and the impact of the WRS on the leak rates were examined.

3.5.1   DP-01 Leak Rate Comparisons

A comparison of the DP-01 leak rate predictions from the PFM codes and from AFEA with the LEAPOR code is shown in Figure 3-38. Figure 3-39 compares the AFEA with LEAPOR predictions with the xLPR, PRObability of Loss Of Coolant Accident (PROLOCA), and Probabilistic Methods for Evaluating and Understanding Structures (PROMETHEUS) code predictions. The PROLOCA and PROMETHEUS comparisons were added because these codes also use the same Henry-Fauske thermohydraulic model and crack morphology parameters to calculate the leak rate. The AFEA predictions with LEAPOR match well with the PROLOCA predictions up to about 37 months. Afterwards, the AFEA with LEAPOR prediction rapidly increases, whereas PROLOCA predicts several months of slowly increasing leak rates before a rapid increase. The xLPR code predictions follow the AFEA results up to 32 months. Afterwards, the leak rate increases steadily up to 44 months in the xLPR code.

Figure 3-38   DP-01 AFEA with LEAPOR leak rates compared to PFM code calculations

Figure 3-39   DP-01 AFEA with LEAPOR leak rates compared to xLPR, PROLOCA, and PROMETHEUS code calculations

No differences in the leak rate trends were observed. Figure 3-40(a) shows the AFEA-predicted crack shape for DP-01 right after through-wall penetration, and Figure 3-40(b) shows the crack shape 14 months later. Right after through-wall penetration, the crack shape looks like a transitioning crack, where the outside diameter length is small but there is still a semi-elliptical shape. Fourteen months later, the crack shape is very close to idealized, although it is technically not an idealized TWC.

(a)   **(b)**
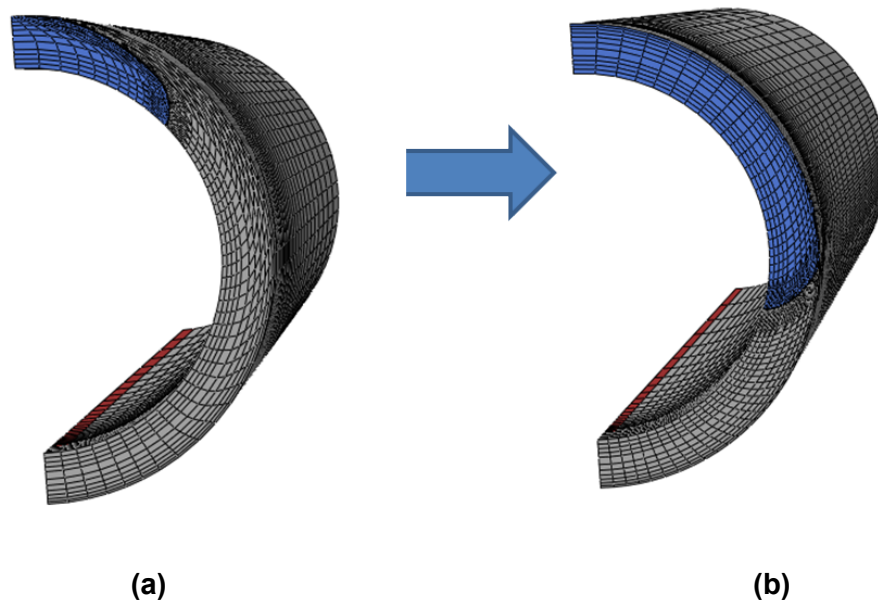
Figure 3-40   DP-01 finite element mesh of crack shape (a) right after TWC formation and (b) 14 months later

3.5.2   DP-02 Leak Rate Comparisons

A comparison of the DP-02 leak rate predictions from the PFM codes and from AFEA with LEAPOR code is shown in Figure 3-41. Figure 3-42 compares the AFEA with LEAPOR code predictions with the xLPR, PROLOCA, and PROMETHEUS code predictions. These figures show that the leak rate trend predicted by AFEA with LEAPOR code is much different than the trends predicted by the PFM codes. The PFM codes predict a rapid increase in the leak rate immediately after the crack penetrates through-wall. However, AFEA with the LEAPOR code predicts that the time from a TWC to a 10 gpm (0.63 kg/s) leak rate will be approximately 26 months, and it will take about another 20 months to reach 50 gpm (3.15 kg/s). In comparison, the xLPR code predicts 8 and 1 months for the same points.
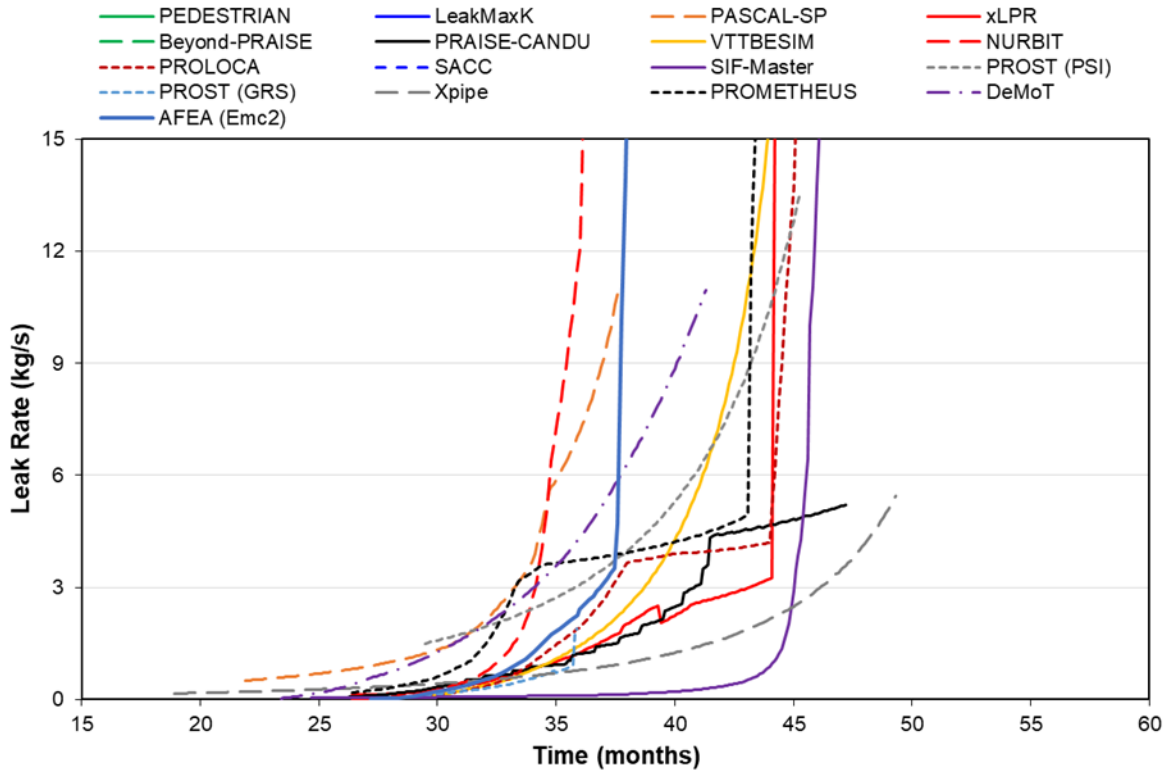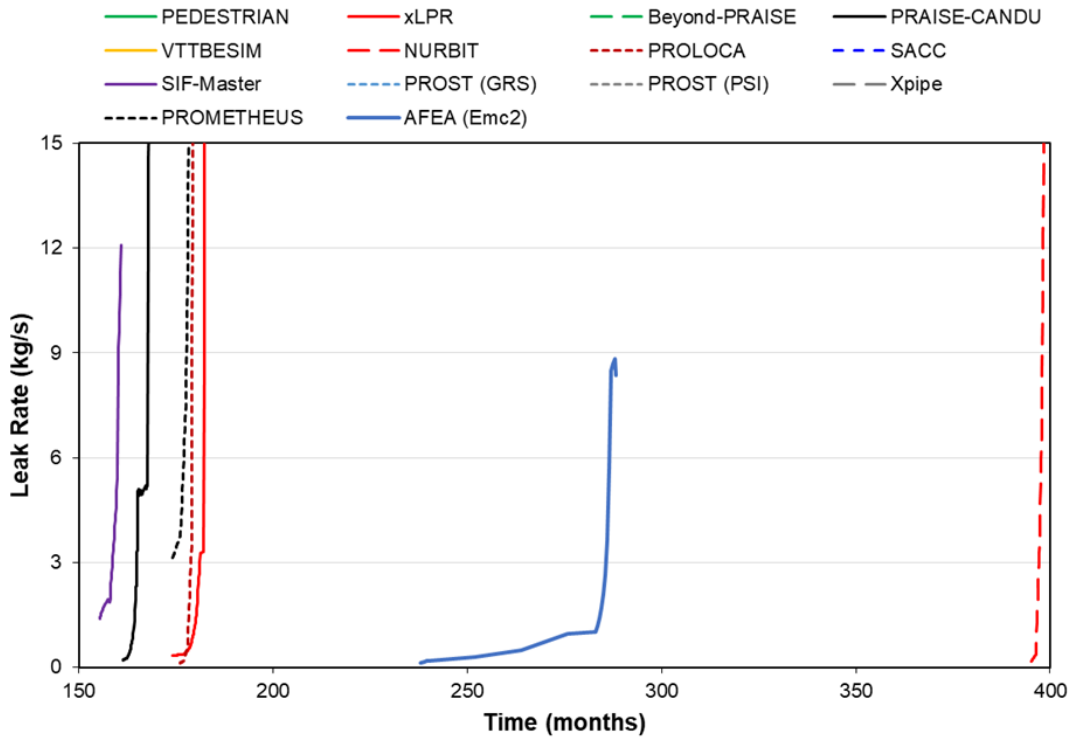
Figure 3-41   DP-02 AFEA with LEAPOR code leak rates compared to PFM code calculations
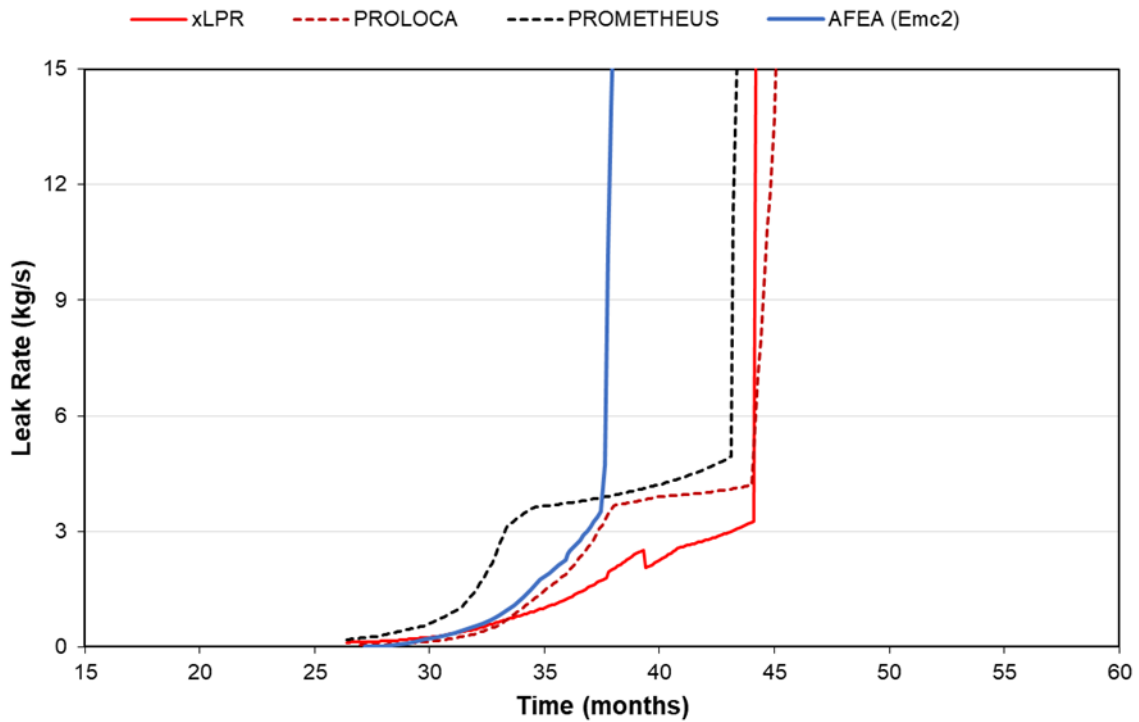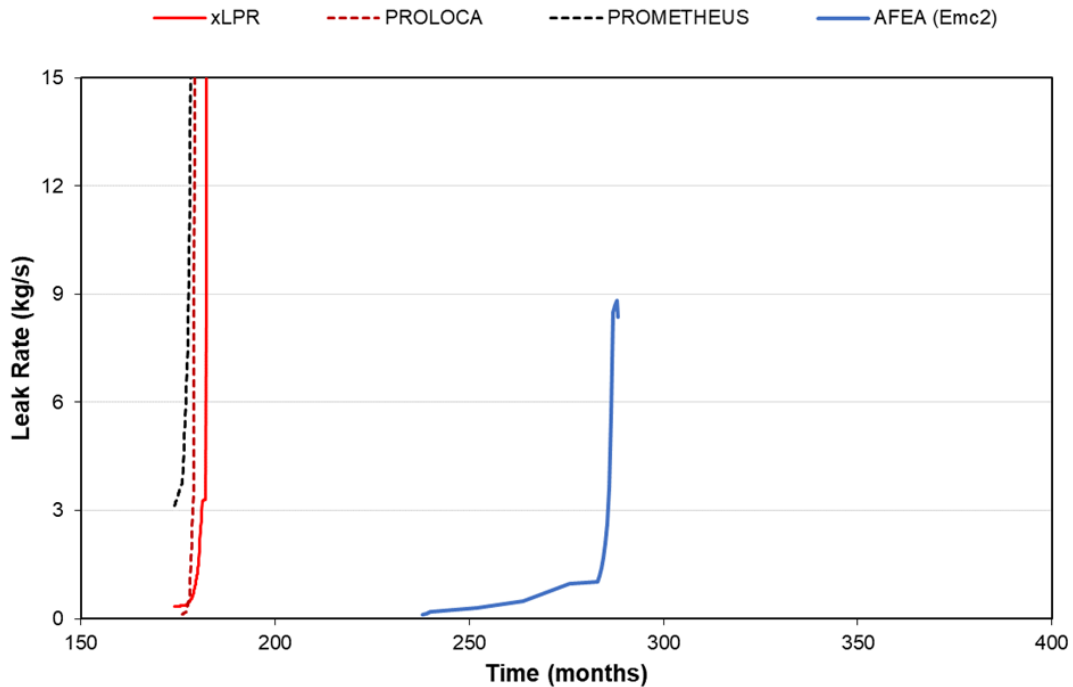
Figure 3-42   DP-02 AFEA with LEAPOR code leak rates compared to xLPR, PROLOCA, and PROMETHEUS code calculations

The differences in the calculated leak rates, especially among the xLPR, PROMETHEUS, and PROLOCA codes, which all use the same leak rate model, can be linked to the different crack shape predictions. As discussed in Section 3.4.2, the DP-02 CODs on both the inside and outside diameters show a similar trend to the leak rate predictions. The outside diameter crack length results for DP-02 show a similar trend.

Figure 3-43(a) shows the AFEA-predicted crack shape for DP-02 right after becoming a TWC, and Figure 3-43(b) shows the crack shape 48 months later. When the crack becomes a TWC, the inside diameter length is quite long, which makes the crack shape far from idealized. While the PFM codes may also predict this type of crack shape and account for it in their crack transition models, when the crack moves out of the transitioning phase an idealized crack shape is assumed. However, Figure 3-43 shows that AFEA predicts a complex crack shape 48 months after through-wall penetration. As a result, there is more time between (a) TWC formation and detectable leak, and (b) detectable leak to rupture. This behavior is further discussed in Section 3.6.

| (a) | (b) |
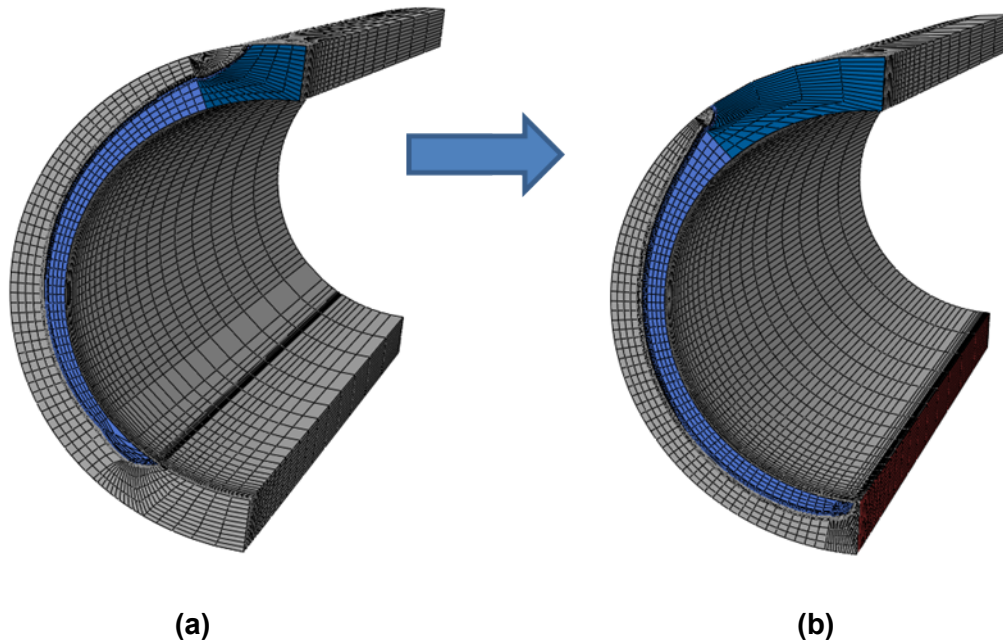
Figure 3-43   DP-02 finite element mesh of crack shape (a) right after TWC formation and (b) 48 months later

3.6   Critical Crack Size

The stability of a crack determines when pipe rupture will occur. If the critical crack size has been reached, then it is assumed that the crack is no longer stable and that the pipe has ruptured. The critical crack size can be calculated three different ways using the AFEA results. The first way uses the LBB.ENG2 method develop by Brust, et al. [11]. Since the WRS does not impact the critical crack size in the LBB.ENG2 calculations, the predicted critical crack size using this method is the same for both DP-01 and DP-02. The LBB.ENG2 method predicts a critical crack size of 64.5 percent of the circumference. The second way to determine the critical crack size uses an elastic perfectly plastic analysis to calculate the critical crack size. Such an analysis is akin to a limit load solution, but the finite element method is used. This method was explored for both DP-01 and DP-02; however, it predicted unrealistically large crack sizes. The third way to determine the critical crack size is to apply the full stress-strain curve to a given crack size and perform FEA, ignoring crack growth, to determine the fracture toughness, J. When J exceeds the initiation fracture toughness, J_{Ic} (in this case 528 N/mm for the weld metal as reported in the Inputs Group Report, issued 2017 [12]), the crack is unstable and the critical crack size has been reached[1]. Figure 3-44 shows the full stress-strain curve that was applied for this approach for both DP-01 and DP-02.

---

[1] For such an analysis, crack growth is ignored because the J-resistance curve is a function of crack growth; therefore, a lower bound critical crack size is predicted.
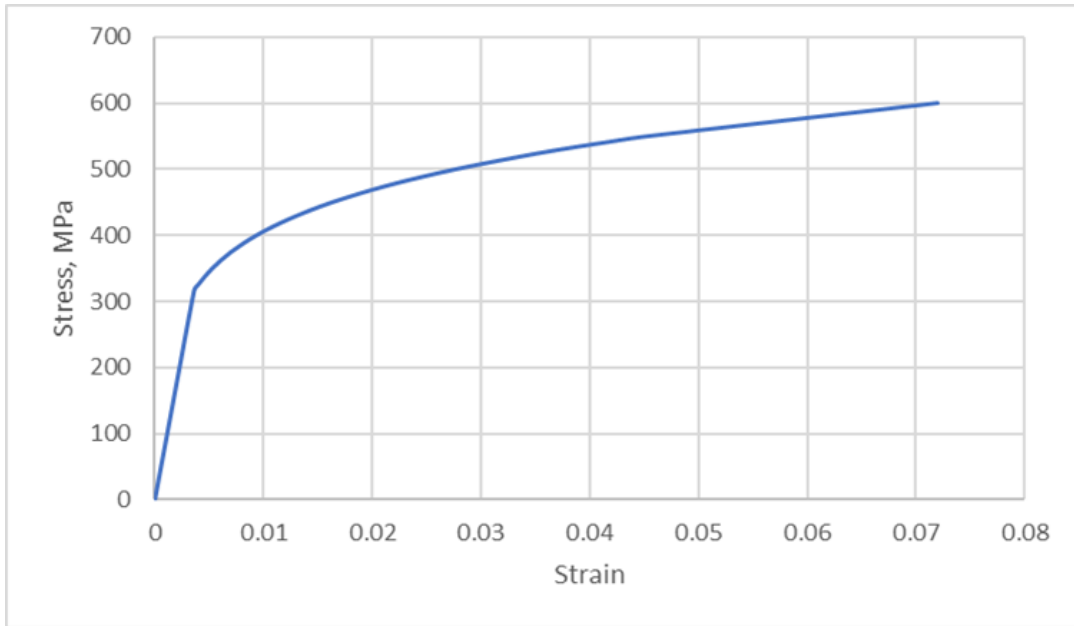
Figure 3-44   Full stress-strain curve used for crack stability predictions

It is noted that the AFEA methods for determining the critical crack size are based on J-integral tearing and are different than the net-section collapse method specified for the PFM codes in the benchmark. This difference should be considered when interpreting the comparisons of the critical crack sizes among the PFM code and AFEA predictions in Sections 3.6.1 and 3.6.2.

3.6.1   DP-01 Critical Crack Size Comparisons

Table 3-1 shows the DP-01 critical crack size predictions from the PFM codes and AFEA predictions using the full stress-strain curve with critical crack size based on J_{Ic}. The percent difference from the AFEA prediction is shown for each of the PFM codes. Note that θ_i and θ_o represent the inside and outside diameter crack half-length angles, respectively. AFEA predicted a normalized average crack length of 56.15 percent of the circumference (i.e., average of 59.9 percent on the inside diameter circumference and 52.4 percent on the outside diameter circumference). As the table shows, the AFEA predictions are close to many of the PFM code predictions. This outcome was expected because the AFEA-predicted crack shape for DP-01 is like the idealized crack shape assumed in the PFM code models.

Table 3-1   DP-01 critical crack size comparisons

Prediction	θ_i/π	θ_o/π	Average[2] Percent Difference from AFEA
PEDESTRIAN	0.581	0.581	3%
PROLOCA (Emc²)	0.55	0.536	-3%
PROLOCA	0.55	0.536	-3%
PROLOCA (PSI)	0.551	0.536	-3%
PROMETHEUS	0.577	0.575	3%
PROST (PSI)	0.595	0.525	0%
PROST (GRS)	0.525	0.525	-7%
LeakMaxK	0.525	0.525	-7%
PASCAL-SP	0.54	0.54	-4%
xLPR	0.587	0.587	5%
DeMoT	0.03	0.223	-77%
Beyond-PRAISE	0.512	0.512	-9%
PRAISE-CANDU	0.509	0.509	-9%
VTTBESIM	0.527	0.466	-12%
SACC	0.567	0.447	-10%
NURBIT	0.618	0.54	3%
SIF-Master	0.471	0.408	-22%
Xpipe	0.525	0.525	-7%
AFEA	0.599	0.524	-

3.6.2   DP-02 Critical Crack Size Comparisons

Table 3-2 shows the DP-02 critical crack size predictions from the PFM codes and AFEA predictions using the full stress-strain curve with the critical crack size based on J_{Ic}. Like before, the percent difference from the AFEA predictions is also shown for each of the PFM codes. The critical crack size predicted by AFEA was 43 percent of the circumference on the outside diameter and 100 percent on the inside diameter. The only PFM code that predicted a 360-degree surface crack on the inside diameter was NURBIT. Due to the differences in crack shape, there is much greater variability in the critical crack size predictions for DP-02. No critical crack size comparisons were made for PROST(GRS), PROST(PSI), SACC, VTTBESIM, and Xpipe because these PFM codes all predicted break-before-leak behavior, and thus there was no TWC data to analyze.

---

[2] Average of the differences at the inside and outside diameters.

Table 3-2   DP-02 critical crack size comparisons

Prediction	θ_i/π	θ_o/π	Average Percent Difference from AFEA
PEDESTRIAN	0.495	0.570	-26%
PROLOCA	0.531	0.520	-27%
PROMETHEUS	0.581	0.580	-19%
xLPR	0.584	0.584	-18%
Beyond-PRAISE	0.532	0.492	-28%
PRAISE-CANDU	0.532	0.495	-28%
NURBIT	1	0.385	-3%
SIF-Master	0.469	0.285	-47%
AFEA	1	0.430	-

3.7   Comparison to Probabilistic Benchmark Results

The benchmark study included several probabilistic comparisons that built upon DP-02 with some selected inputs having their uncertainties represented by probability distributions. Since AFEA is a deterministic analysis, it would not be computationally practical to run it within a Monte Carlo structure. Therefore, the mean or median values from the probabilistic results for the PP-01 benchmark problem were compared to the AFEA results. The median values were expected to be like the deterministic results from the PFM codes.

Figure 3-45 shows the probability distribution functions from several of the PFM codes for the probability of leak (i.e., development of a TWC) for PP-01. The median value can be read directly from quantile 0.5 on the vertical axis. The mean values of the times to TWC formation are represented by the yellow dots. The AFEA result is shown by the orange vertical line. The mean values of TWC formation as predicted by the PFM codes ranged from 180 to 420 months; however, only one PFM code predicted TWC formation past 280 months. With removal of this outlier prediction, the range in PFM codes predictions is 180 to 280 months. AFEA predicted a TWC at 240 months, which is close to the average of the PFM code mean predictions. The median values are more representative of the results from DP-02. The AFEA prediction for DP-02 lies between the 50th and 80th percentiles of the distributions generated by the PFM codes. The exception was the NURBIT code, where the AFEA prediction lies at the 20th percentile.
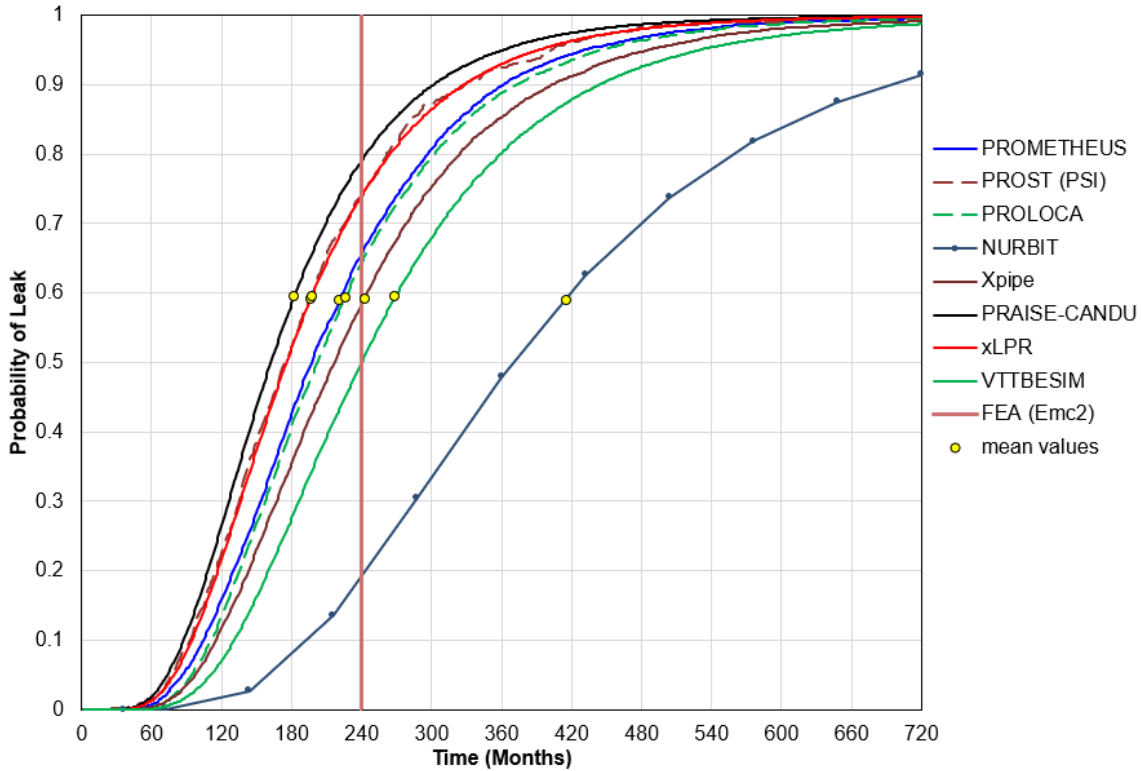
Figure 3-45 PP-01 probability of leak calculated by PFM codes compared to DP-02 AFEA calculation

Table 3-3 shows the differences between the median and the mean values from each of the PFM codes and the AFEA prediction. Based on these comparisons, many of the PFM codes have reasonable predictions for the probability of leak. NURBIT has the biggest differences, not only in its mean and median values compared to the AFEA predictions, but also in its probabilistic predictions as compared to the other PFM codes as seen in Figure 3-45. The two PFM codes that are most like the AFEA prediction are VTTBESIM and Xpipe.

Table 3-3 Difference in median and mean PFM code predictions from AFEA results

Code	Median Difference from AFEA Prediction (yr)	Mean Difference from AFEA Prediction (yr)
PROMETHEUS	-3.58	-1.57
PRO-LOCA	-3.17	-1.13
NURBIT	+10.83	+14.67
Xpipe	-1.92	+0.25
PROST (PSI)	-5.50	-3.65
PRAISE-CANDU	-6.50	-4.80
xLPR	-5.33	-3.53
VTTBESIM	-0.00	+2.42

4 CONCLUSIONS

In this study, AFEA results were leveraged to inform assessment of the xLPR code's performance in the international PFM code benchmark study. Assessment of the xLPR code's performance in the benchmark study and relative to the AFEA results will guide future maintenance and development needs to ensure that the xLPR code is consistent with or leads the state-of-practice.

Even among the PFM code comparisons, there were differences in the DP-01 and DP-02 results, which highlight the importance of WRS in the crack growth and subsequent leak rate and crack stability calculations. AFEA also highlighted the importance of WRS on crack shape development. Since the AFEA procedure determines the SIFs at every point along the crack front and then uses those values to determine crack growth over time for each node point, it is possible to develop a crack shape in AFEA that is much different than the basic crack shapes supported by the PFM codes. The PFM codes typically assume an idealized crack shape. Even for those PFM codes, like xLPR, that include a crack transition model, a non-idealized crack shape is only modelled during the transition phase of crack growth. As described in Section 3.5, drastically different crack shapes were not seen in DP-01 where the WRS profile was linear. However, drastically different crack shapes were seen in DP-02 where the third-order polynomial WRS profile with the highly compressive stress at the mid-thickness allowed a long crack to develop along on the inside surface while still allowing the crack to grow slowly through the thickness of the weld. Based on these results, further investigation could be pursued on the impact of the WRS on the crack shape and how well the crack growth models, including the transition model, can capture non-idealized crack shapes. Nevertheless, with respect to modeling complex crack shapes, the xLPR code is generally consistent with the PFM code state of practice.

The ability to model non-idealized crack shapes can be important in predicting failure criteria, such as the time from TWC to detectable leak and the time from detectable leak to rupture. The differences among the PFM code and AFEA predictions for these periods of crack evolution emphasize the impact that accurately modeling the crack shape can have on the calculated response time. In cases where some of the PFM code results better matched the AFEA results, it is recommended to analyze the approaches used by the other PFM codes to determine what, if any, features might be beneficial to include in future versions of the xLPR code. It would also be beneficial to compare an AFEA with xLPR code results using a WRS profile in which the universal weight function method can be utilized.

Crack shape development also affects the COD calculations. The COD comparisons among the AFEA and the PFM code predictions, while exhibiting some differences, showed similar trends for DP-01. However, the AFEA predictions for DP-02 were quite different from the PFM code predictions. The WRS clearly impacted the CODs on both the inside and outside diameters in the AFEA predictions, and this effect was not observed in the PFM codes. The effects of WRS could either be directly a result of the stress or indirectly through its impact on the crack length, which then affects the predicted COD as discussed in Section 3.4.2. The PFM code predictions

also showed differences in how quickly the COD increased, which suggests that there may be other factors such as the idealized crack assumption that are impacting the predicted COD values. The COD is the primary variable in determining the leak rate, and the slower AFEA-predicted COD increases after TWC penetration in DP-02 led to much longer times between a detectable leak and rupture than the PFM code predictions. Some analyses have been completed to determine an analytical factor that could be applied to account for the WRS effects on the COD calculations as described in [7]. A maintenance request has been submitted to include this effect in the xLPR code.

In summary, the xLPR code generally performed well relative to AFEA and the other PFM codes involved in the benchmark study. Accordingly, within the parameters of these studies, the xLPR code is consistent with the state of practice. A challenge was observed for the xLPR code when a surface crack does not preserve the idealized elliptical crack shape. In such cases, it is possible that the estimation of SIFs at additional locations around the crack front could produce results that are closer to the AFEA predictions. Assessing the extent to which the xLPR code may lead the state of practice is more difficult because of the constraints of the benchmark study. For instance, WRS has been shown to be critical in many of the results, and use of the universal weight function method allows the xLPR code to better represent a range of potential WRS profiles. However, to accommodate the capabilities of all the PFM codes, only linear and third-order polynomial WRS profiles were considered. A benchmark problem with a realistic, nonpolynomial WRS profile could reveal the versatility of the xLPR code.

5 REFERENCES

[1] Homiack, M., "Probabilistic Fracture Mechanics Codes for Piping International Benchmark—Part 1: Deterministic Comparisons," PVP2022-84724, in *Proceedings of the ASME 2022 Pressure Vessels & Piping Conference*, Las Vegas, Nevada, July 17-22, 2022.

[2] Shim, D. J., S. Kalyanam, E. Punch, T. Zhang, F. Brust, G. Wilkowski, A. Goodfellow, and M. Smith, "Advanced Finite Element Analysis (AFEA) Evaluation for Circumferential and Axial PWSCC Defects," PVP2010-25162, in *ASME Pressure Vessels & Piping Conference*, Bellevue, WA, 2010.

[3] Rudland, D., D. J. Shim, T. Zhang, and G. Wilkowski, "Implication of Wolf Creek Indications - Final Report," Washington, D.C., August 2007, NRC Agencywide Documents Access and Management System (ADAMS) Accession No. ML072470394.

[4] Brust, F. W., D. J. Shim, G. Wilkowski, and D. Rudland, "PWSCC Crack Growth Modeling Approaches," PVP2011-57974, in *Proceedings of the ASME 2011 Pressure Vessels & Piping Division Conference*, Baltimore, MD, July 17-21, 2011.

[5] NRC, NUREG-0531, "Investigation and Evaluation of Stress-Corrosion Cracking in Piping of Light Water Reactor Plants," Washington, D.C., February 1979, NRC ADAMS Accession No. ML19263D018.

[6] Shim, D. J., R. Kurth, and D. Rudland, "Development of Non-Idealized Surface to Through-Wall Crack Transition Model," PVP2013-97092, in *Proceedings of the ASME 2013 Pressure Vessels and Piping Conference*, Paris, France, July 14-18, 2013.

[7] NRC, Technical Letter Report "Estimation Scheme for Weld Residual Stress Effect on Crack Opening Displacements," September 18, 2020, NRC ADAMS Accession No. ML22124A002.

[8] Henry, R., "The Two-Phase Critical Discharge of Initially Saturated or Subcooled Liquid," *Nuclear Science and Engineering,* vol. 41, pp. 336-342, 1970.

[9] Henry, R. E., H. K. Fauske, and S. T. McComas, "Two-Phase Critical Flow at Low Qualities Part I: Experimental," *Nuclear Science and Engineering,* vol. 41, pp. 79-91, 1970.

[10] Henry, R. E., H. K. Fauske, and S. T. McComas, "Two-Phase Critical Flow at Low Qualities Part II: Analysis," *Nuclear Science and Engineering,* vol. 41, pp. 92-98, 1970.

[11] Brust, F. W. and P. Gilles, "Approximate Methods for Fracture Analysis of Tubular Members Subjected to Combined Tensile and Bending Loads," *Journal of Offshore Mechanics and Arctic Engineering,* vol. 116, pp. 221-227, 1994.

[12] Homiack, M., "xLPR Group Report—Inputs Group, Version 1.0," Washington, D.C., December 19, 2017, NRC ADAMS Accession No. ML19337B876.